land

MDPI

Article

Sub-Watershed Parameter Transplantation Method for Non-Point Source Pollution Estimation in Complex Underlying Surface Environment

Xuekai Chen [1,2,3], Guojian He [1], Xiaobo Liu [2,3,*], Bogen Li [4], Wenqi Peng [2,3], Fei Dong [2,3], Aiping Huang [2,3], Weijie Wang [2,3] and Qiuyue Lian [2,3]

[1] State Key Laboratory of Hydroscience and Engineering, Department of Hydraulic Engineering, Tsinghua University, Beijing 100084, China; chenxk@iwhr.com (X.C.); heguojian@tsinghua.edu.cn (G.H.)
[2] State Key Laboratory of Simulation and Regulation of Water Cycle in River Basin, China Institute of Water Resources and Hydropower Research, Beijing 100038, China; pwq@iwhr.com (W.P.); dongfei@iwhr.com (F.D.); aphuang@iwhr.com (A.H.); wjwang@iwhr.com (W.W.); QiuyueL@163.com (Q.L.)
[3] Department of Water Ecology and Environment, China Institute of Water Resources and Hydropower Research, Beijing 100038, China
[4] Yunnan Hydrological and Water Resources Bureau, Kunming 650106, China; bogenli@163.com
* Correspondence: xbliu@iwhr.com

check for updates

Citation: Chen, X.; He, G.; Liu, X.; Li, B.; Peng, W.; Dong, F.; Huang, A.; Wang, W.; Lian, Q. Sub-Watershed Parameter Transplantation Method for Non-Point Source Pollution Estimation in Complex Underlying Surface Environment. *Land* **2021**, *10*, 1387. https://doi.org/10.3390/land10121387

Academic Editors: Zeyuan Qiu, Subhasis Giri, Amy Teffer, Jennifer Fair, Stephanie Figary and Angelinus Franke

Received: 19 October 2021
Accepted: 12 December 2021
Published: 14 December 2021

Publisher's Note: MDPI stays neutral with regard to jurisdictional claims in published maps and institutional affiliations.

Copyright: © 2021 by the authors. Licensee MDPI, Basel, Switzerland. This article is an open access article distributed under the terms and conditions of the Creative Commons Attribution (CC BY) license (https://creativecommons.org/licenses/by/4.0/).

Abstract: The prevention and control of non-point source pollution is an important link in managing basin water quality and is an important factor governing the environmental protection of watershed water in China over the next few decades. The control of non-point source pollution relies on the recognition of the amount, location, and influencing factors. The watershed nonpoint source pollution mechanism model is an effective method to address the issue. However, due to the complexity and randomness of non-point source pollution, both the development and application of the watershed water environment model have always focused on the accuracy and rationality of model parameters. In this pursuit, the present study envisaged the temporal and spatial heterogeneity of non-point source pollution caused by the complex underlying surface conditions of the watershed, and the insufficient coverage of hydrological and water quality monitoring stations. A refined watershed non-point source pollution simulation method, combining the Monte Carlo analytic hierarchy process (MCAHP) and the sub-watershed parameter transplantation method (SWPT), was established on the basis of the migration and transformation theory of the non-point source pollution, considering the index selection, watershed division, sub-watershed simulation, and parameter migration. Taking the Erhai Lake, a typical plateau lake in China, as the representative research object, the MCAHP method effectively reduced the uncertainty of the weights of the watershed division indexes compared to the traditional AHP method. Furthermore, compared to the traditional all watershed parameter simulation (AWPS) approach, the simulation accuracy was improved by 40% using the SWPT method, which is important for the prevention and control of non-point source pollution in large-scale watersheds with significant differences in climatic and topographic conditions. Based on the simulation results, the key factors affecting the load of the non-point source pollution in the Erhai watershed were identified. The results showed that the agricultural land in Erhai Lake contributed a majority of the load for several reasons, including the application of nitro phosphor complex fertilizer. Among the different soil types, paddy soil was responsible for the largest pollution load of total nitrogen and total phosphorus discharge into the lake. The zones with slopes of 0–18° were found to be the appropriate area for farming. Our study presents technical methods for the assessment, prevention, and control of non-point source pollution load in complex watersheds.

Keywords: non-point source pollution; sub-watershed parameter transplantation method; SWAT; Monte Carlo analytic hierarchy process; underlying surface; influencing factor

1. Introduction

Non-point source pollution has become a major factor leading to the deterioration of water quality in rivers and lakes [1,2], and is an important challenge for the protection of water quality worldwide [3]. In China, agricultural non-point source pollution contributes to about 40–60% of the watershed pollution load [4], and similar situations occurred in the United States in the last decade [5]. Affected by the land use type and distribution [6], rainfall conditions [7], agricultural planting structure [8], and watershed hydrological characteristics [9], the generation and emission of non-point source pollutants are intermittent and random [10], resulting in strong heterogeneity in the temporal and spatial distribution [11]. In China, the prevention and control of non-point source pollution is the key link in the objective management of watershed water quality [12]. The accurate description of the temporal and spatial variation characteristics of watershed non-point source pollution, identification of the primary influencing factors, and implementation of targeted treatment measures are the most effective approaches to watershed water environment treatment in China [13]. Meanwhile, with the influence of economic investment, topographic conditions, and other factors, the hydrological and water quality monitoring stations in China are not uniformly distributed [14]. Even in a watershed, the runoff and pollution generation can be misinterpreted due to the heterogeneous spatial distribution of the monitoring stations [15]. Therefore, the establishment of a refined simulation method for watershed non-point source pollution in the current monitoring network is immensely important for the realization and management of watershed water quality in China.

For the acquisition of more accurate watershed non-point source pollution results, over the last 60 years, the watershed non-point source pollution models have developed from the original single hydrological process simulation to the current systematic simulation of watershed hydrology and nutrient circulation. The conceptual models have evolved into physical models. The Soil Water Assessment Tool (SWAT) was mainly used to simulate the water quality and quantity of surface water and to analyze the impact of complex underlying surface conditions on hydrology, sediment, and nutrient circulation in a watershed. Compared with the previous non-point source pollution models, the hydrologic research unit (HRU) was taken as the compute unit in the SWAT model for calculations [16], and the simulation efficiency was significantly improved. The SWAT has achieved fruitful research results in different fields, such as the impact of climate change and human activities [17–19], the impact of land use change [20–22], hydrological circulation simulation [23–25], sediment loss calculation [26–28], discussion on the law of nutrient loss [2,29,30], assessment of the impact on the ecological environment [31–33], and the evaluation of optimized management measures for non-point source pollution [34,35]. In China, the SWAT models have also been applied in important regions such as the Yangtze River watershed [36], the Three Gorges Reservoir Area [37,38], and Taihu Lake [39]. SWAT models have achieved satisfactory results in both application fields and adaptation.

In the scope of the occurrence mechanism of non-point source pollution, the migration and transformation of nutrients such as nitrogen and phosphorus are differently affected by the meteorology, underlying surface, and other factors. The nutrient circulation processes can be generalized into a mathematical equation following the mechanism models, and the simulation accuracy can be adjusted with hundreds of modeling parameters [40]. Therefore, whether the input of model parameters can characterize the spatial differences of these important influencing factors greatly determines the applicability of the models [41,42]. If the watershed is divided into many smaller watersheds and simulated stepwise with the mechanism models, accurate simulation results can be obtained. However, the workload significantly increases, especially in the context of complex river networks and water systems. In contrast, since the simulation results are the comprehensive embodiment of many adjusted parameters, the phenomenon of "different parameters leading to the same effect" usually occurs, and it is difficult for the selected parameters to be representative [43]. In addition, the current hydrological and water quality monitoring stations in China do not support this methodology. Currently, when mechanism models are applied to simulate

non-point source pollution in the watershed, the whole-watershed parameter simulation methods are commonly adopted [44]. In fact, the locally limited water quantity and water quality monitoring data were used to determine the key parameters of all subordinate watersheds, and thereby the non-point source pollution load of the entire watershed was obtained. However, for large-scale watersheds, especially those with large topographic fluctuations and significant spatial formula climate characteristics, the determination of many parameters is usually unreasonable, resulting in the inability of the optimal local simulation to truly reflect the variation characteristics of the non-point source pollution in the entire watershed.

In view of this background, the sub-watershed parameter transplantation (SWPT) method developed in the present study is expected to solve the issue of determining the non-point source pollution model parameters in complex watersheds with limited monitoring data. In this method, the watershed was divided according to the hydrological, meteorological, topographic, and geomorphic factors of the whole watershed. Based on data availability and other conditions, typical sub-watersheds were selected in each division, and these sub-watersheds were finely simulated following the model. After quantification and verification of the accuracy, the representative parameter groups were obtained. These groups were popularized and simulated in each division, and then the simulation results in each division were summarized to derive the non-point source pollution load of the whole watershed. The SWPT method has the advantages of mechanism simulation and can fix the drawback of lack of data measured, therefore simulation results with high accuracy can be obtained. Considering the lack of data, Cheng Yan et al. [45] and Wu Biqiong et al. [46] applied the parameter transplantation method to simulate the hydrological and nutrient circulation processes in the region of Jialing River without the data. The results showed that the transplantation of hydrological parameters had good applicability, and the transplantation of parameters, related to nitrogen and phosphorus pollutants, could be popularized; however, the simulation accuracy was low. Hong Qian et al. [47] constructed a sub-watershed parameter extension method to divide the Three Gorges Reservoir region, and typical sub-watersheds were selected for the simulation. Subsequently, the parameter extension method was adopted to simulate the changes in the agricultural non-point source pollution in the Three Gorges Reservoir area. The research results showed that the sub-watershed parameter extension method significantly improved the simulation accuracy of the non-point source pollution in the watershed, indicating the necessity of applying the sub-watershed parameter extension method in relatively complex watersheds. However, in the watershed dividing system, topographic indexes alone were taken as the dividing basis, and the representativeness of the divisions was controversial.

As a typical plateau lake in China, the Erhai Lake is the second largest freshwater lake in Yunnan Province. The Erhai Lake watershed covers an area of 2565 km^2, with elevations between 1960 m and 4040 m. The altitude difference is up to 2000 m, with an obvious gradient. The watershed contains 8 land use types and 25 soil types, and almost one million people in 19 towns live there. The watershed plays an important role in regional hydrological circulation, ecosystem stability, and social and economic development [48]. Meanwhile, the water environment of Erhai Lake is under great pressure from the rapid development of the regional social economy. The lake is at the state of an important inflection point in the early stage of eutrophication [49]. Therefore, with continuous reinforcement and improvement of point source pollution treatment in the watershed, the reduction in non-point source pollution load in the watershed will be crucial. In this study, considering the spatial heterogeneity of the climate and underlying surface conditions in the Erhai Lake watershed, the representative indicators affecting the generation and transport of non-point source pollution were selected, and the dividing methodology of the Erhai lake watershed was established on the basis of the Monte Carlo-based AHP (MCAHP) method. Based on the dividing results, the typical sub-watersheds in each division were selected as the important research objects, and the SWAT model was adopted to carry out refined hydrological and nutrient circulation simulations for the

typical sub- watersheds to obtain the representative parameter groups in each division. Meanwhile, the division parameter transplantation method was compared with the all-watershed parameter simulation (AWPS) method to further elucidate the necessity of adopting the SWPT for complex watersheds. Finally, the effects of different underlying surface conditions on the pollution load into the lake were discussed, and the important underlying surface threshold values affecting the load of non-point source pollution in the Erhai Lake watershed were screened. Our work provides the theoretical and technical scaffold for the establishment of efficient and targeted watershed non-point source pollution control schemes.

2. Materials and Methods

2.1. Study Area and Date Availability

The Erhai Lake watershed is located in Dali City and Eryuan County, Yunnan Province, China, and belongs to the Lancang River watershed. It has an area of 2565 km^2 and a population of 400/km^2, and is situated at an altitude of 1960–4040 m (Figure 1a). At the normal water level of 1974 m (Yellow Sea elevation), the lake has an area of 249.8 km^2, an average water depth of 10.5 m, and a storage capacity of 28.8 × 108 m^3. The meteorological conditions of the watershed include an annual average temperature of 16.4°C, the annual average precipitation and evaporation are 784 mm and 1127 mm, respectively, and the annual sunshine is 48.80%. In terms of the hydrological conditions, there are 28 main rivers flowing into the lake: MJ, YA, and LS in the north, 18 creeks of Cangshan in the west, FW, YL, HD, and XH in the east, and BL in the south of the watershed. The location and elevation of the study area are shown in Figure 1a, as well as the precipitation (Figure 1b), slope (Figure 1c), vegetation coverage (Figure 1d), and sub-watershed (Figure 1e). The data used in this study are listed in Table 1. Considering the completeness of the data and the social and economic development of the basin, this study selects 2013–2017 as the research period.

Table 1. Date type scale and data description.

Data Type	Scale	Source	Data Description
Elevation	1:250,000	Geospatial Data Cloud. Available online: http://www.gscloud.cn (accessed on 13 November 2021)	Sub-watershed division basis, geographic elevation, slope, slope length in 2015
Soil type	1:1,000,000	Institute of Soil Science, Chinese Academy of Sciences	Classification of soil types and physicochemical properties of soil in 2010
Land use type	1:100,000	Remote sensing image interpretation	Classification of land use types in 2016
Meteorological	13 stations	China Meteorological Data Network (http://data.cma.cn, accessed on 13 November 2021)	Precipitation, temperature, evaporation, wind speed, relative humidity, solar radiation from 2013 to 2017
Hydrology and water quality		Dali Branch of Yunnan Hydrology and Water Resources Bureau	Physical and chemical indexes such as river discharge, nitrogen and phosphorus from 2013 to 2017
Socioeconomic data		Dali Prefecture Agriculture Bureau	Crop planting type, planting and harvest time. Fertilization type, time and amount from 2013 to 2017
Water conservancy project	Three medium-sized reservoirs	Dali Branch of Yunnan Hydrology and Water Resources Bureau	Reservoir capacity, operating water level, inbound and outbound flow, and water quality from 2013 to 2017

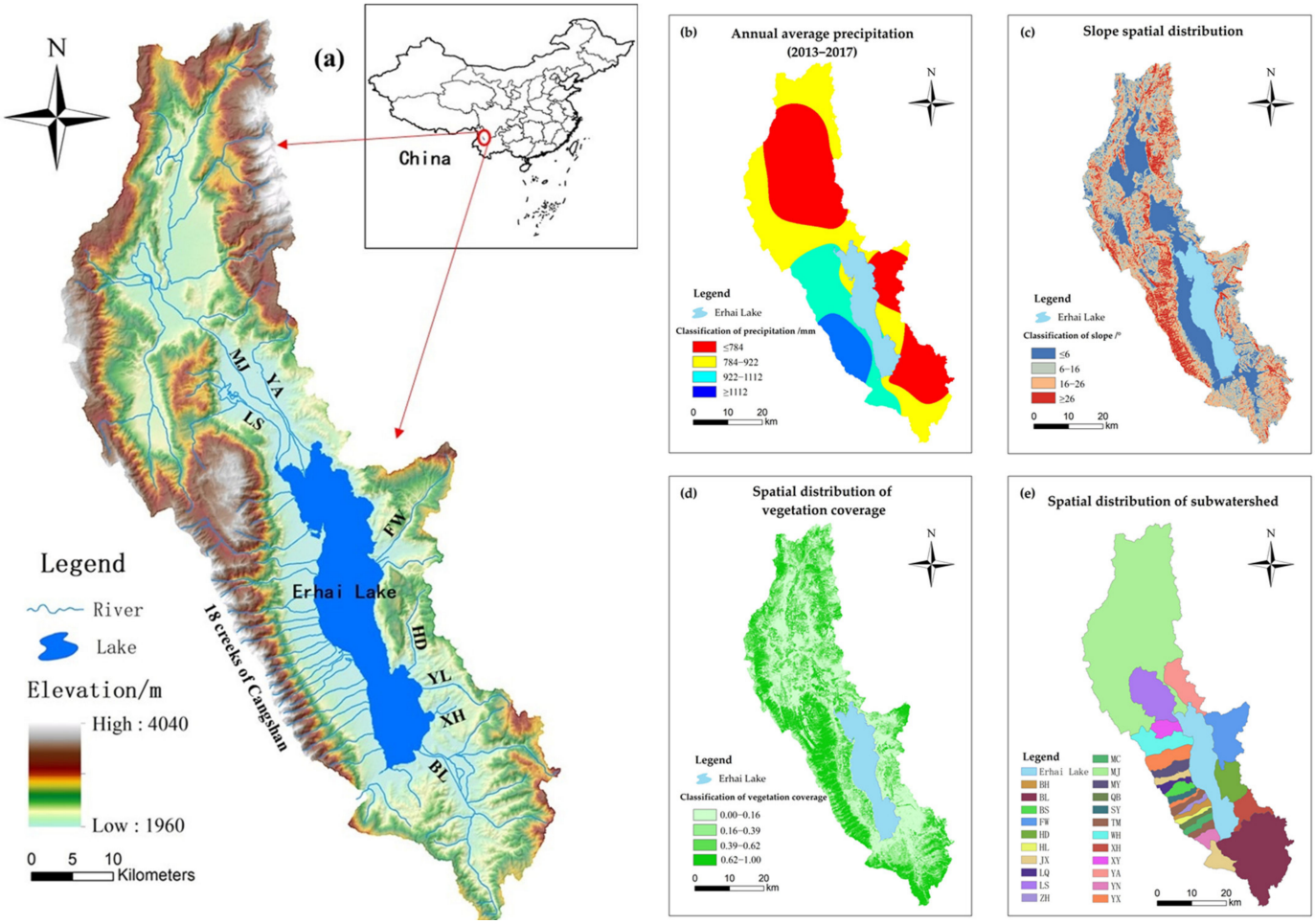


Figure 1. Elevation (**a**), precipitation (**b**), slope (**c**), vegetation coverage (**d**), and sub-watershed (**e**) of the Lake Erhai watershed.

2.2. Sub-Watershed Parameter Transplantation (SWPT)

Based on appropriate parameters obtained in typical sub-watersheds, simulations were performed in the mechanism model by extending these parameters to the entire watershed. Three research foci were selected for this method: (1) the selection of dividing indexes, (2) the division of the watershed, and (3) simulation following the mechanism model.

2.2.1. Dividing Index

The selection of reasonable dividing indexes is the basis of the division parameter transplantation method. Based on previous research, the primary factors affecting the migration and transformation of non-point source pollution included precipitation, geographical elevation, slope, and vegetation coverage, which were selected as the dividing indexes in this study. Precipitation and topography are important factors affecting the generation and transport of non-point source pollution, and both play a key role in non-point source pollution [50,51], especially in plateau lake watersheds with evident spatial differences in climate and large topographic fluctuations. Rainfall intensity principally has an impact on the load and nutrient concentration peak time, while the rainfall duration has a significant impact on the loss of pollutants. The slope is an important factor affecting pollutant migration, and the contents of dissolved nitrogen and phosphorus in runoff are affected by the slope through the influence on runoff. Vegetation canopy has significant effects on infiltration, surface runoff, and evapotranspiration. In addition, the precipitation in the Erhai Lake watershed increased with the elevation of altitude, and the change in

the vertical direction was significant [52]. This phenomenon is particularly obvious in the west and north of Erhai Lake. If the average altitude was increased by 100 m, the average precipitation could increase by 47 mm.

Based on GIS, the indexes were spatially rasterized, and the dividing indexes were classified according to the sample mean—mean square deviation method [53]. The equations are expressed as follows:

$$\overline{R} = \frac{1}{n} \cdot R_i \tag{1}$$

$$S = \sqrt{\frac{1}{n-1} \cdot \sum_{i=1}^{n} (R_i - \overline{R})^2} \tag{2}$$

where R_i is the grid attribute parameters, including precipitation (mm), elevation (m), slope (°), and vegetation coverage (dimensionless); $\overline{R}$ represents the mean of grid attribute parameters; and S is the mean square deviation of the grid attribute parameters. Taking the mean value $\overline{R}$ as the center and S as the mean square deviation, the dividing indexes can be divided into the following four groups: $(-\infty, \overline{R}-S)$, $(\overline{R}-S, \overline{R})$, $(\overline{R}, \overline{R}+S)$, and $(\overline{R}+S, +\infty)$, which represent the ranges of precipitation, elevation, slope, and vegetation coverage, respectively.

2.2.2. Watershed Delineation

Based on the levels of indexes and index weight results, the superposition of multiply indexes in the divisions can be calculated as follows:

$$S_i = \alpha_P \cdot P_i + \alpha_E \cdot E_i + \alpha_D \cdot D_i + \alpha_V \cdot V_i \tag{3}$$

where S_i represents the score of grid i evaluated; and α_P, α_E, α_D, and α_V denote the weights of precipitation, elevation, slope, and vegetation coverage indexes, respectively. The weights were quantified according to the descriptions in Section 2.3. P_i, E_i, D_i, and V_i correspond to the scores of precipitation, elevation, slope, and vegetation coverage indexes, respectively.

In the GIS environment, the functions of the grid layer calculator and division statistics script were adopted to carry out the superposition and fusion of multiple indexes. Finally, the spatial map of the divided watersheds was generated.

2.2.3. Mechanism Model

In this study, the SWAT model, which is the most widely applied non-point source pollution simulation and assessment model, was selected as the physical mechanism model. This model is composed of 701 equations and 1013 intermediate variables. In the GIS operating environment, DEM, land use type, soil type, meteorological data, agricultural planting mode, etc., were taken as the input parameters, with HRU as the basic calculation unit, for the simulations of critical processes such as hydrological circulation, soil erosion, and nutrients (such as nitrogen and phosphorus) circulation in agricultural watersheds. The SWAT model has the advantages of high operation efficiency, accessibility of input data, and continuous temporal simulation.

In this study, the rationality of the simulation results was tested with the correlation coefficient (R^2) and the Nash–Sutcliffe efficiency coefficient (*Ens*), which can be calculated according to formulas (4) and (5).

$$R^2 = \frac{\sum_{i=1}^{n} (Y_i^{obs})^2 - \frac{1}{n} \sum_{i=1}^{n} (Y_i^{obs})^2}{\sum_{i=1}^{n} (Y_i^{sim})^2 - (\frac{1}{n} \sum_{i=1}^{n} Y_i^{sim})^2} \tag{4}$$

$$Ens = 1 - \frac{\sum_{i=1}^{n} (Y_i^{obs} - Y_i^{sim})^2}{\sum_{i=1}^{n} (Y_i^{obs} - Y_i^{mean})^2} \quad (5)$$

where Y_i^{obs} stands for the ith value measured; Y_i^{sim} represents the ith value simulated; Y_i^{mean} stands for the mean value measured; and n denotes the number of values measured.

2.3. Monte-Carlo-Based AHP Algorithm (MCAHP)

Determining the weights of the dividing indexes is crucial for the rationality of the dividing results. In this study, the MCAHP was developed using the MATLAB operating platform. The beta-PERT distribution function was introduced in this algorithm [54], and thereby the problem of a large uncertainty of index weight caused by the limited input data in traditional AHP methods was resolved. The calculation procedures are described as follows:

Step 1: For the dividing indexes selected, according to the Saaty proportional relationship defined in formula (6), the comparison matrix *PCM* of element a_{ij} was constructed. The non-diagonal elements in *PCM* were generally scored by experts.

$$\begin{gathered} PCM = [a_{ij}] \\ a_{ij} > 0,\ a_{ij} = 1/a_{ji},\ a_{ij} = a_{ji} = 1\ (i = j) \end{gathered} \quad (6)$$

Step 2: For the non-diagonal elements in *PCM*, the corresponding beta distribution was generated on the basis of the minimum (min), maximum (max), and most possible value (modal) as scored by experts. The PERT distribution was used to calculate the average value (mean) and standard deviation (stdev) of the non-diagonal elements. The expressions are shown in formulas (7) and (8). These input parameters are indispensable for shape indicators (such as α and β) in the corresponding beta PERT distributions. The parameters were calculated according to formulas (9) and (10).

$$\text{mean} = \frac{\min + 4\text{modal} + \max}{p} \quad (7)$$

$$\text{stdev} = \frac{\max - \min}{p} \quad (8)$$

$$\alpha = \left(\frac{\text{mean} - \min}{\max - \min}\right)\left(\frac{(\text{mean} - \min)(\max - \text{mean})}{\text{stedv}^2} - 1\right) \quad (9)$$

$$\beta = \left(\frac{\max - \text{mean}}{\text{mean} - \min}\right) \cdot \alpha \quad (10)$$

where p represents the number of experts participating in scoring.

Step 3: Random numbers were generated using the random number generator in MATLAB. The beta-PERT distribution of random numbers corresponding to each non-diagonal element a_{ij} of *PCM* was generated.

$$\text{random } a_{ij} = \min + \text{betarnd}(\alpha, \beta) \cdot (\max - \min) \quad (11)$$

where betarnd represents the beta-PERT distribution function established by MATLAB, and its value was calculated according to the shape indexes α and β in the range of 0–1.

Step 4: For each randomly generated *PCM*, formula (12) presents the relationship between the maximum eigenvalue (λ_{max}) and its corresponding eigenvector (W). The eigenvector obtained was further normalized to calculate the relative weight of the dividing index.

$$[PCM][W] = \lambda_{\max}[W] \quad (12)$$

where λ_{max} stands for the maximum eigenvalue of *PCM*, and W is the eigenvector corresponding to λ_{max}.

Step 5: The consistency index (*CR*) was calculated to reflect the consistency degree of the evaluation and to determine the quality of the evaluation matrix. The index was calculated according to formulas (13) and (14). In general, *CR* values smaller than 0.1 are acceptable.

$$CI = \frac{\lambda_{max} - n}{n - 1} \tag{13}$$

$$CR = \frac{CI}{RI} \tag{14}$$

where *CI* is the average random consistency index.

Step 6: The aforementioned calculation procedures were repeated 100 to 10,000 times. The normalized weights of different index layers or criterion layers with respect to the target layer were obtained by a kernel smoothing method, and the corresponding probability density function was drawn.

Based on the constructed division parameter migration method, the research framework of this paper is shown in Figure 2.

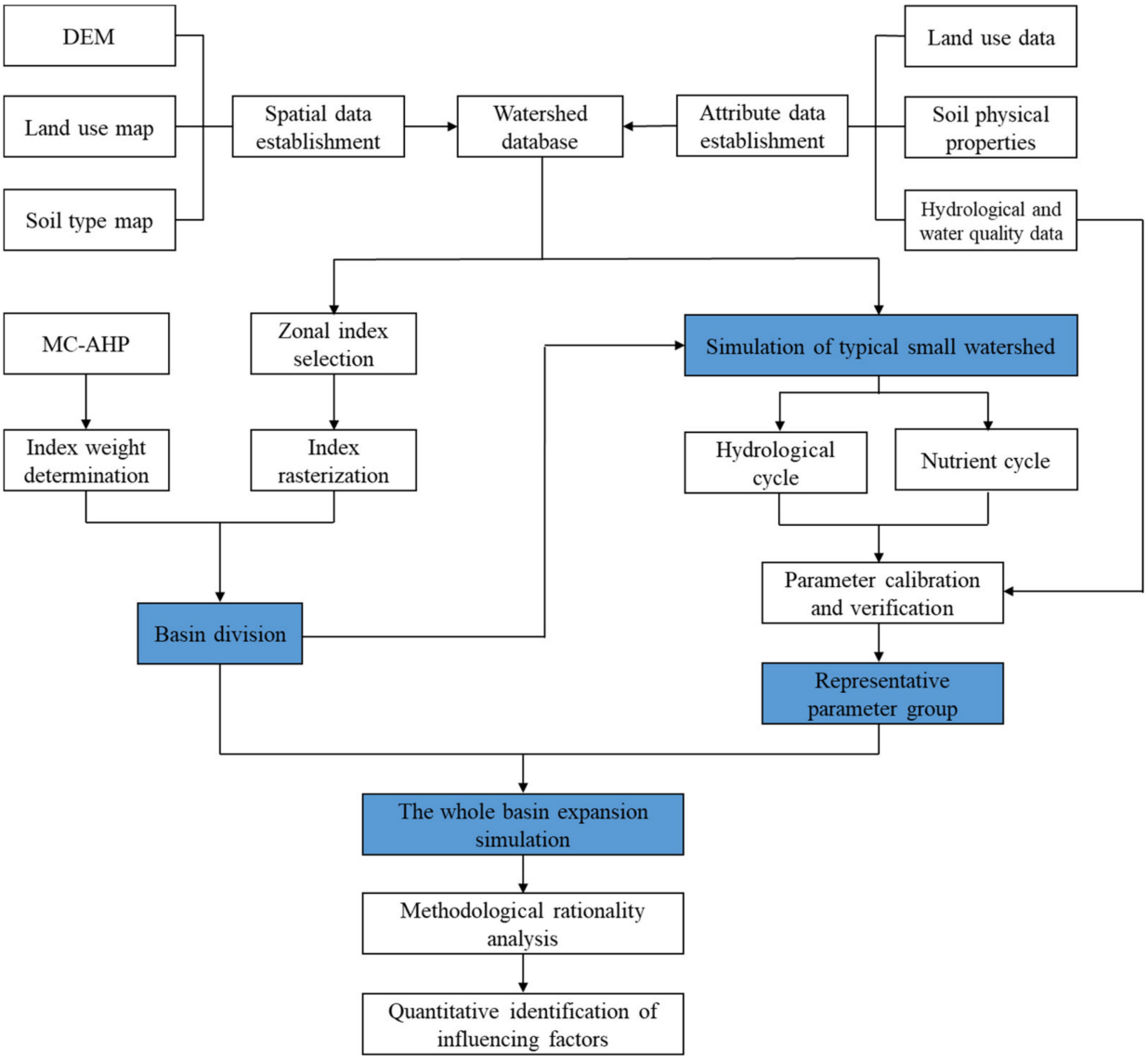


Figure 2. Study framework.

3. Results and Analysis

3.1. Determination of Weight of Dividing Index

According to formulas (6) and (14), the calculations were repeated 1000 times to obtain the *CR* calculation results of the index matrixes. All *CR* values were smaller than 0.1 (Figure 3), indicating that the results of the evaluation matrixes were acceptable. The probability distribution density of the index weight derived by the kernel smoothing method was plotted in Figure 4a. The precipitation and slope indexes had relatively high weights, followed by vegetation coverage and elevation indexes. Figure 4b shows the 95% confidence intervals of the weights obtained by the AHP and MCAHP methods. Compared to AHP, the MCAHP method tended to concentrate the weight near the mean and control it within a small confidence interval. The beta-PERT distribution significantly reduced the standard deviation of the index weight and minimized the error due to subjective judgment as much as possible.

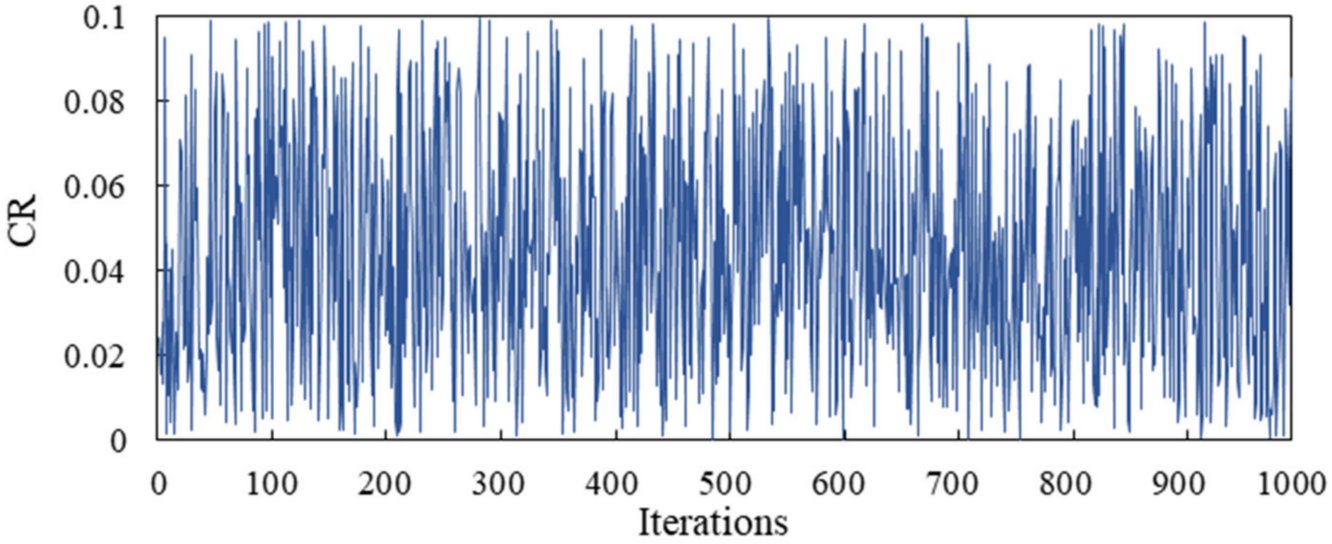


Figure 3. *CR* calculation results of MCAHP.

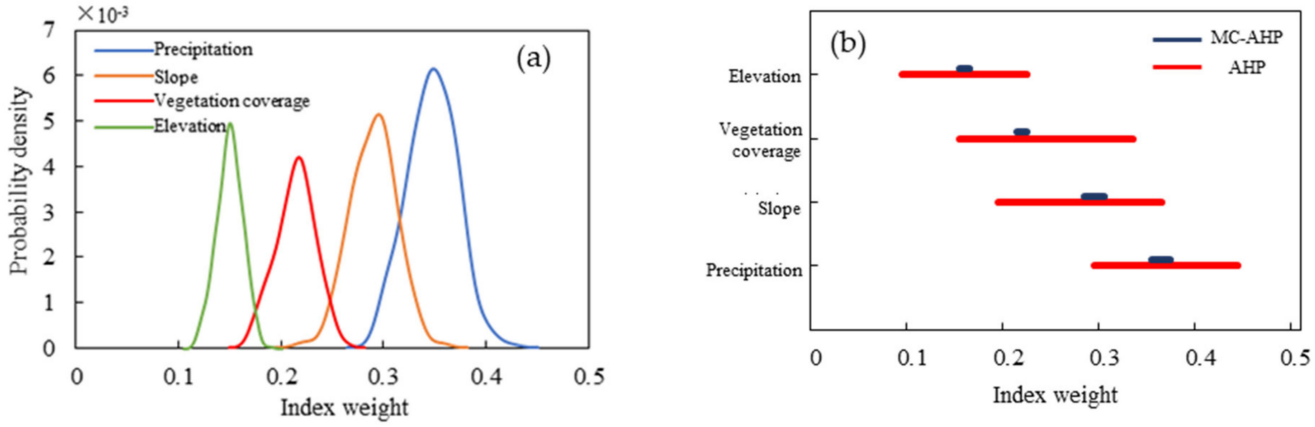


Figure 4. Determination of weight of dividing index: Probability density distribution of index weight (**a**), 95% confidence intervals for index weights (**b**).

3.2. Watershed Division and Selection of Sub-Watersheds

Based on the dividing index system and watershed dividing method, with the subordinate watersheds as the basic units, the Erhai watershed was divided into four regions (Figure 5a), including the Eryuan flatland river region in the north (hereinafter referred to as the north region), the Dali high mountain river region in the west (west region), the

Fengyi middle-height mountain river region in the south (south region), and the Haidong low mountain river region in the east (east region). After the statistical analysis of the precipitation, landform, and vegetation coverage in each division of the watershed (Table 2), it was recognized that the spatial differences in the climate and the underlying surface conditions of different divisions were significant. The precipitation in the west region was significantly higher than that in other divisions. In addition, the rivers were short in this region, so it was easier for the non-point source pollutants to access the water body of the lake. The average altitudes and average slopes in the north and west regions were greater than those in other regions, and thereby the migration and transformation of pollutants were accelerated. The vegetation coverage in the east region was relatively low, and the loss phenomenon for water and soil was more serious. As a result, a large amount of particulate pollution was adsorbed on sediment granules, and the pollutants, along with the granules, entered the water body.

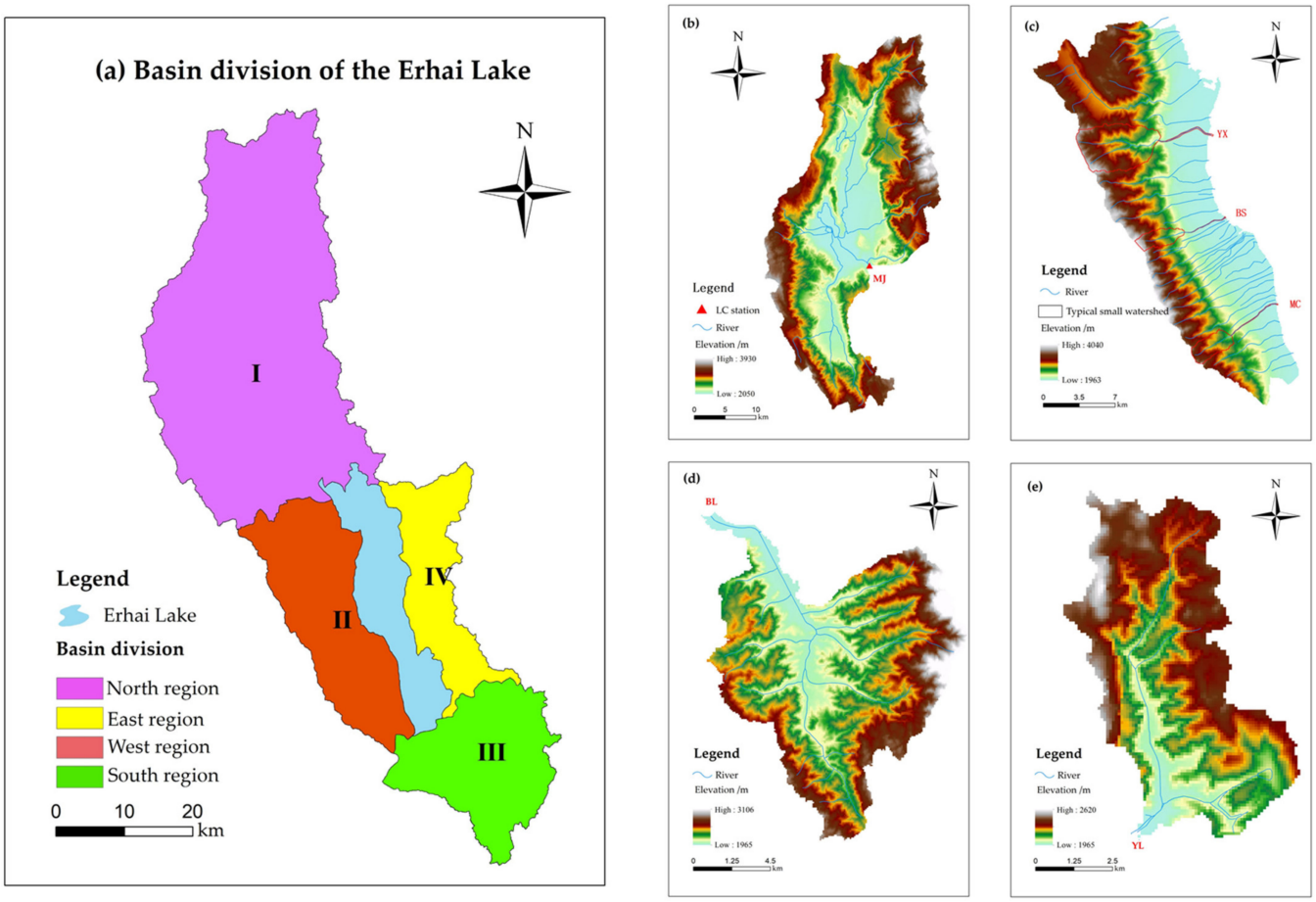


Figure 5. Watershed division and selection of sub-watersheds. Basin division of the Erhai Lake (**a**), the watershed upstream of the LC station of the MJ (**b**), YX, BS, and MC watershed in the west region (**c**), BL watershed in the south region (**d**), and YL watershed in the east region (**e**).

Table 2. Zone overview of Lake Erhai watershed.

Zone	Average Precipitation/mm	Average Elevation/m	Average Slope/°	Average Vegetation Coverage
North	790.7	2631.0	13.89	0.34
West	1097.1	2587.4	18.95	0.48
South	804.5	2283.2	12.95	0.38
East	773.5	2225.2	11.88	0.24

Considering the integrity of monitoring the data and representativeness of geographical locations, based on the dividing results, the MJ in the north, YX, BS, and MC in the west, BL in the south, and YL in the east were chosen as the representative sub-watersheds, and their spatial distributions are shown in Figure 5b–e. The watershed upstream of the LC station of the MJ accounts for 80.18% of the entire MJ watershed, and covers all land use types and 80% of soil types in the Eryuan flatland river region in the north. This watershed controls approximately 80% of the MJ flow rate discharged into the lake. The LC station possessed continuous water quantity and quality monitoring data, meeting the parameter calibration requirements of the model. The water quantity from YX is the largest among the 18 rivers in the Cangshan mountain, so its model parameters were highly representative. The BS is located in the middle of the west region and possessed continuous monitoring data. The MC is located in the south of the west region, with a large pollution load. The BL area is the region with the most concentrated cities and towns in the Erhai Lake watershed, and the human activities are closest to Erhai Lake. The YL is the largest river discharged into the lake in the east region.

3.3. Simulation of the Sub-Watersheds

The Latin hypercube method (LH-OAT) in the SWAT model was used for the sensitivity analysis of relevant parameters such as flow rate, nitrogen, and phosphorus. The results are shown in Table 3. The flow rate parameters among these regions were significantly different. The north region was dominated by the natural river water systems, and CN2, ALPHA_BF, and SURLAG were the most sensitive parameters. The west and south regions were greatly affected by human activities and were frequently exchanged with groundwater, and ALPHA_BFBF was the most sensitive parameter. The vegetation coverage in the east region was low, with serious loss of water and soil. The physical and chemical properties of the soil were the key factors influencing the runoff, and CN2, SOL_AWC, and SOL_K were the most sensitive parameters. With respect to the nitrogen and phosphorus parameters, the parameter sensitivity among the different regions was similar.

Table 3. Parameter sensitivity analysis of SWAT model in Lake Erhai.

Variable	North		West		South		East	
	Parameter	**Rank**	**Parameter**	**Rank**	**Parameter**	**Rank**	**Parameter**	**Rank**
Flow	CN2.mgt	1	ALPHA_BF.gw	1	ALPHA_BF.gw	1	CN2.mgt	1
	ALPHA_BF.gw	2	SLSUBBSN.hru	2	CN2.mgt	2	SOL_AWC.sol	2
	SURLAG.bsn	3	CH_N2.rte	3	CH_K2.rte	3	SOL_K.sol	3
	GW_REVAP.gw	4	CN2.mgt	4	SLSUBBSN.hru	4	ALPHA_BF.gw	4
	CH_N2.rte	5	SOL_AWC.sol	5	SOL_AWC.sol	5	ESCO.hru	5
P	SOL_ORGP.chm	1	SOL_ORGP.chm	1	SOL_ORGP.chm	1	SOL_ORGP.chm	1
	SOL_SOLP.chm	2	SOL_SOLP.chm	2	SOL_SOLP.chm	2	SOL_SOLP.chm	2
	PPERCO.bsn	3	PPERCO.bsn	3	PPERCO.bsn	3	PPERCO.bsn	3
N	CDN.bsn	1	CDN.bsn	1	SOL_ORGN.chm	1	SOL_OGRN.chm	1
	SDNCO.bsn	2	SDNCO.bsn	2	CDN.bsn	2	SOL_NO3.chm	2
	SOL_OGRN.chm	3	SOL_OGRN.chm	3	SDNCO.bsn	3	NPERCP.bsn	3

Note: CN2: SCS moisture condition II curve number for pervious areas; ALPHA_BF.gw: baseflow recession constant; SURLAG: surface runoff lag coefficient; GW_REVAP: revap coefficient; CH_N2: Manning value for the main channel; SOL_AWC: available water capacity; CH_K2: effective hydraulic conductivity of channel; SOL_K: saturated hydraulic conductivity of first layer; ESCO: soil evaporation compensation coefficient; SOL_ORGP: initial humic organic phosphorus in soil layer; SOL_SOLP: initial soluble P concentration in soil layer; PPERCO: phosphorus percolation coefficient; CDN: rate coefficient for denitrification; SDNCO: threshold value of nutrient cycling water factor for denitrification to occur; SOL_ORGN: initial humic organic nitrogen in soil layer; SOL_NO3: initial NO_3 concentration in soil layer; NPERCP: nitrate percolation coefficient.

In this study, 2013 was set as the warm-up period, 2014–2015 was set as the calibration period of the model, and 2016–2017 was set as the validation period of the model. Flow, total nitrogen (TN), ammonia nitrogen (NH_3-N), and total phosphorus (TP) were selected as simulation indicators. The R^2 and *Ens* were adopted to evaluate the rationality of the model parameter calibration and verification of the results. The calibration and verification procedures of each division are shown in Figure 6, and the statistical results of the model rationality are shown in Table 4. Regardless of the flow rate and water quality simulations, the R^2 values of typical sub-watersheds were greater than 0.8, and the *Ens* values were greater than 0.7, except for the YL. The R^2 and *Ens* values of YL were relatively low, as this area was affected by the point source pollution in flood seasons. In general, the Erhai representative sub-watersheds SWAT model constructed in this study showed good applicability in the simulation of flow rate and non-point source pollution.

Table 4. Calibration and validation of SWAT model simulation parameters in sub-watersheds.

River	Variable	Calibration		Validation	
		R^2	*Ens*	R^2	*Ens*
MJ	Flow	0.92	0.91	0.88	0.85
	NH_3-N	0.77	0.71	0.73	0.72
	TP	0.89	0.80	0.88	0.71
YX	Flow	0.94	0.91	0.88	0.84
	TN	0.86	0.78	0.74	0.71
	TP	0.82	0.80	0.79	0.79
BS	Flow	0.90	0.85	0.86	0.81
	TN	0.83	0.81	0.79	0.76
	TP	0.81	0.78	0.83	0.76
MC	Flow	0.92	0.90	0.88	0.83
	TN	0.86	0.75	0.87	0.78
	TP	0.85	0.78	0.91	0.81
BL	Flow	0.94	0.93	0.83	0.83
	TN	0.85	0.85	0.88	0.81
	TP	0.92	0.87	0.88	0.84
YL	Flow	0.74	0.70	0.70	0.63
	TN	0.88	0.62	0.83	0.58
	TP	0.66	0.63	0.59	0.53

3.4. Extended Simulation

Furthermore, the parameter groups of representative sub-watersheds were extended to the entire watershed to simulate the water quantity discharged into the lake and the pollution load of the Erhai Lake watershed. The simulation results were compared with the statistical values of water quantity and pollution load to verify the reliability of the simulation results. In this study, the water quantity data from 2014 to 2017 and pollution load data from 2015 to 2017 were analyzed. The results are shown in Figure 7. The relative errors of water quantity discharged into the lake, TN, and TP were controlled at levels of about 5%, 10%, and 20%, respectively. In general, the SWPT-based simulation results of hydrology and non-point source pollution in the Erhai Lake watershed were reasonable and reliable.

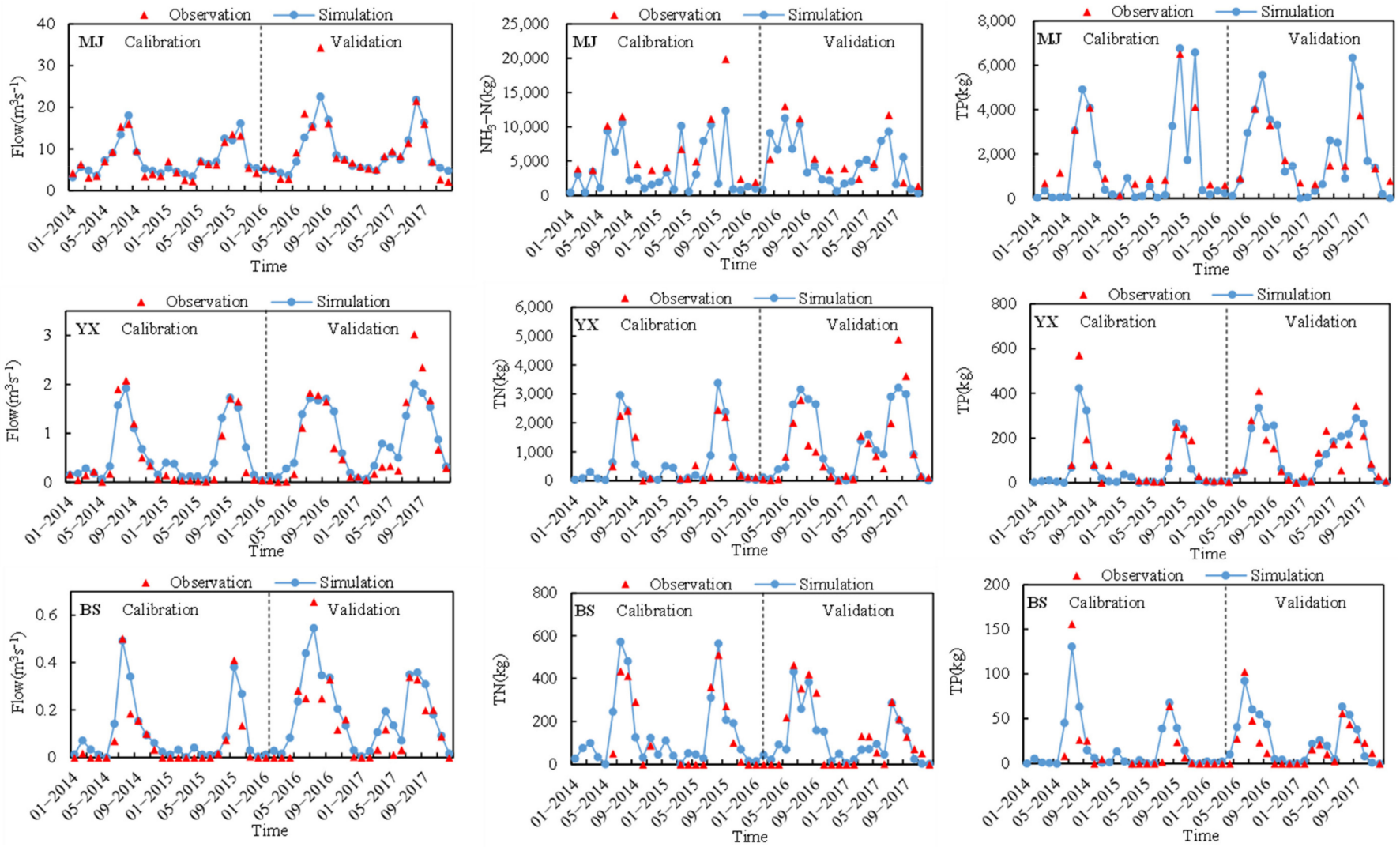


Figure 6. *Cont.*

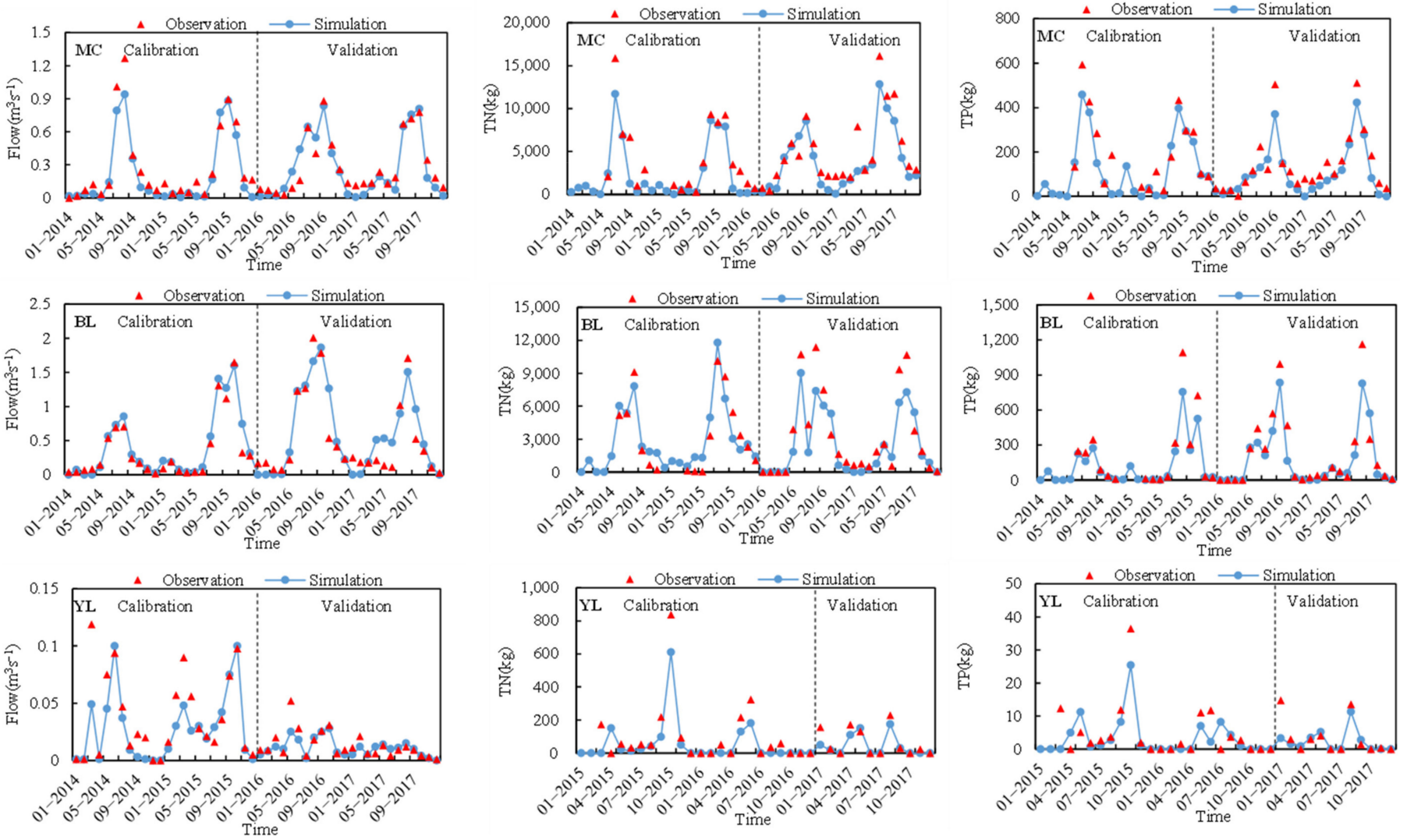


Figure 6. Calibration and validation of runoff, nitrate, and TP in typical sub-watersheds.

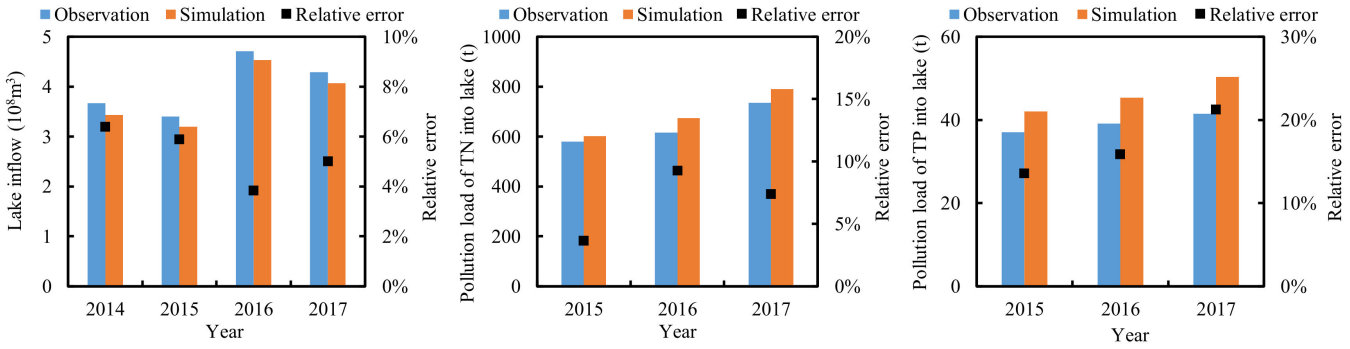


Figure 7. Comparison between simulated and observed values of lake inflow and pollution load in Lake Erhai watershed.

4. Discussion

4.1. Rationality Analysis of the Method

For the verification of the rationality of the SWPT, two simulation schemes were established in this study for comparison. The first scheme adopted the SWPT, while the other adopted the AWPS, in which the division of the watershed was absent, and the optimal simulation results of the water quantity and quality at a certain point were used to determine the parameters. The simulation results of both schemes were obtained, and the reasonability of the division parameter transplantation method was assessed according to the real measured values.

Taking the optimal simulation parameters of MJ as an example, the YX and BL rivers were selected for verification. The SWPT and AWPS methods were separately adopted for the simulations. Figure 8 shows the verification results of both schemes. Irrespective of the regions, the R^2 and *Ens* values of the SWPT were obviously larger than those of AWPS, indicating that the SWPT-based simulation results were more consistent with the real situations. In addition, the results demonstrated that the SWPT could more accurately reflect the impact of the spatial differences of the climate and underlying surface on watershed hydrology and non-point source pollution simulation.

4.2. Identification of Influencing Factors

4.2.1. Land Use

Based on the simulation results, the TN and TP pollution load intensities from forest land, farmland (dry land and paddy field), grassland, construction land, shrub, and bare land in the Erhai watershed are shown in Figure 9. The TN and TP pollution load intensities were ranked as follows: farmland (2.45 and 0.18 kg/ha), construction land (1.89 and 0.15 kg/ha), shrub (1.15 and 0.10 kg/ha), grassland (0.86 and 0.07 kg/ha), forest land (0.72 and 0.06 kg/ha), and bare land (0.32 and 0.04kg/ha). In general, the vegetation coverage of forest land and grassland was relatively high, so the scouring effect of rainwater on the soil was effectively weakened. The root system could effectively fix nutrients. Therefore, the load intensities contributed from the forest land and grassland were relatively low. Due to the influence of the tillage, fertilization, vegetation coverage, and other factors, the load intensity of farmland was significantly higher than those of other land use types. In addition, due to the double-cropping farming system implemented in the Erhai watershed, the land tillage loosened the soil and microorganisms exhibited a strong decomposition activity, resulting in the retention of the residual nutrients on the soil surface and the decomposition of a large quantity of the crop residue. These reasons, along with unreasonable fertilization measures, led to the large load intensity contributed by the farmland. The construction land also contributed to a large extent. Due to land hardening, the land surface runoff fluctuated along with rainstorms, eliminating the adsorption effect of soil for nutrients. In addition, the high-intensity discharge of sewage from residents

also contributed to the high load intensity of construction land. This phenomenon was particularly obvious in the downstream area of the west region.

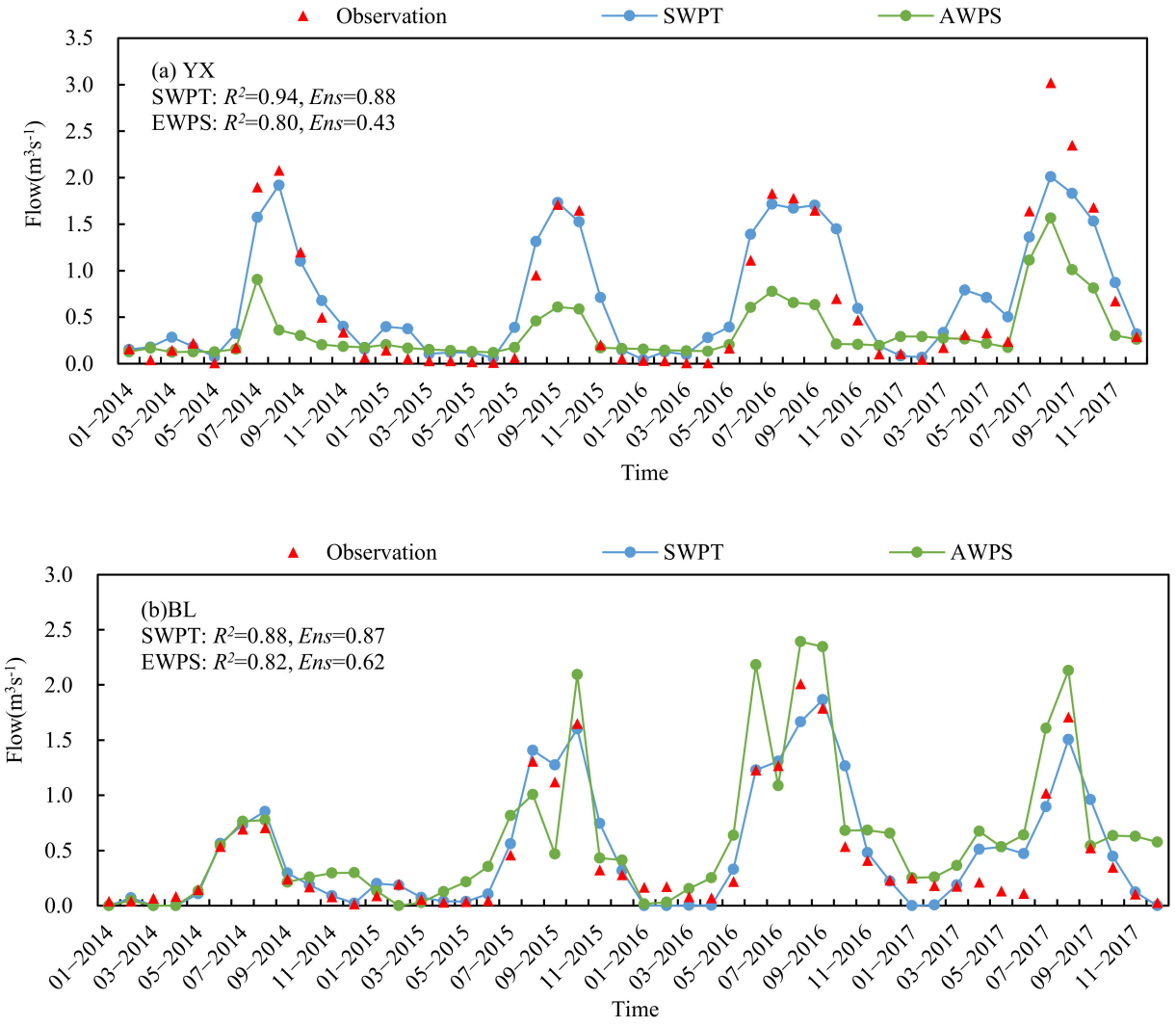


Figure 8. Rationality analysis of SWPT: YX watershed (**a**) and BL watershed (**b**).

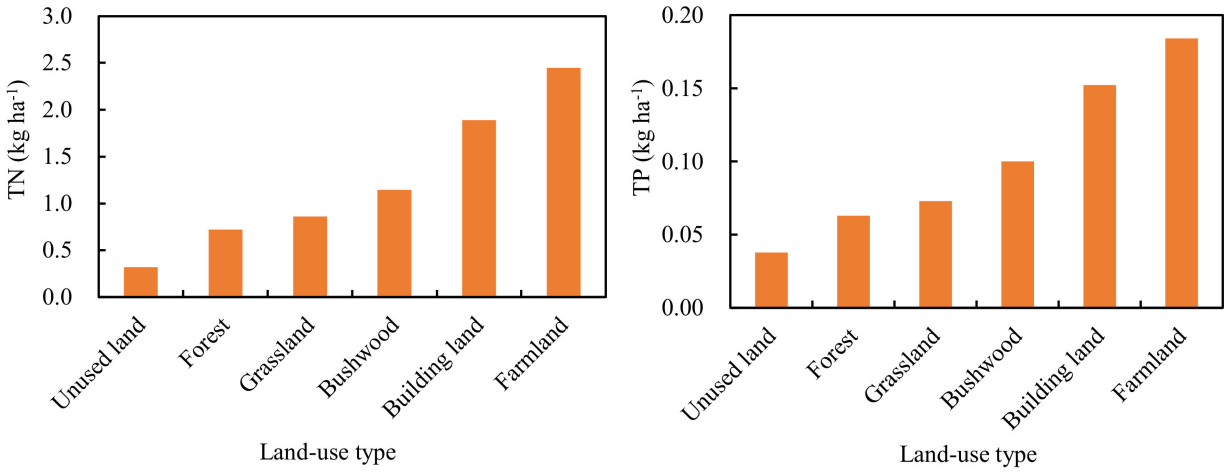


Figure 9. Pollution load intensity of different land use types in Lake Erhai watershed.

4.2.2. Soil

The primary soil types in the Erhai watershed include red soil, yellow-brown soil, and southern paddy soil. Figure 10 shows the TN and TP pollution load intensities in the lake from different soil types in subordinate watersheds. The pollution load intensities from the different soil types were distinct. In detail, the load intensities from the yellow floating mud field (4.59 and 0.25 kg/ha), mud field (3.29 and 0.27 kg/ha), river floating mud (3.42 and 0.19 kg/ha), yellow-red mud (2.77 and 0.18 kg/ha), green mud field (2.06 and 0.16 kg/ha), and clay field (2.02 and 0.17 kg/ha) were relatively high. The reasons for this phenomenon include the following: first, the laterite belonged to the red soil and was distributed in the plateau flat section at altitudes of 1700–2100 m. Among the various soil types in the Erhai watershed, laterite occupied the largest area, accounting for 10.38% of the total area of the watershed. The large area led to the large pollution load of laterite into the lake. Second, yellow floating red mud, mud field, green mud field, and clay field belonged to the paddy soil, which was suitable for crop cultivation and contained copious nitrogen and phosphorus. According to the data, the total nitrogen content in the yellow floating red mud, mud field, green mud field, and clay field was 0.130, 0.170, 0.181, and 0.159%, respectively, and the total phosphorus content was 0.169, 0.186, 0.154, and 0.234%, respectively. These reasons and the influence of artificial fertilization led to the large pollution load intensities of these soil types into the lake. Third, the river floating mud belonged to the newly deposited soil type and was distributed in the river floodplain and terrace of the Erhai watershed. The river floating mud is principally composed of fine and silty sand. The yellow-red mud belonged to red soil and was distributed in the middle and lower sections of the mountains and gentle sections at the piedmonts with elevations of 1400 to 2100 m. These two soil types were relatively loose and belonged to class B in the hydrological grouping, which were prone to water and soil loss with the scouring of precipitation. In general, the different soil types exhibited different pollution load intensities into the lake, which depended on the physical and chemical properties of the soil and human activities.

4.2.3. Slope

According to the slope classification principles in the General Rules for Comprehensive Treatment Planning for Soil and Water Conservation (GB/T 15772-2008), the Erhai Lake watershed was divided into five zones with different slope ranges of 0–8°, 8–15°, 15–25°, 25–35°, and >35°. The TN and TP pollution load intensities into the lake in all of the zones are shown in Figure 11. The TN and TP pollution load intensities of the zone with slopes of 0–8° reached maximums of 1.76 and 0.53 kg/ha, respectively. Noticeably, with the increase of slope, the corresponding pollution load intensities did not increase. The main reason for this phenomenon is that the zones with different slope ranges contained different land use types. For a deep understanding of the influence of slope on nutrient load, the load intensities contributed from the same land use type with different slopes were studied and are described in the following paragraph.

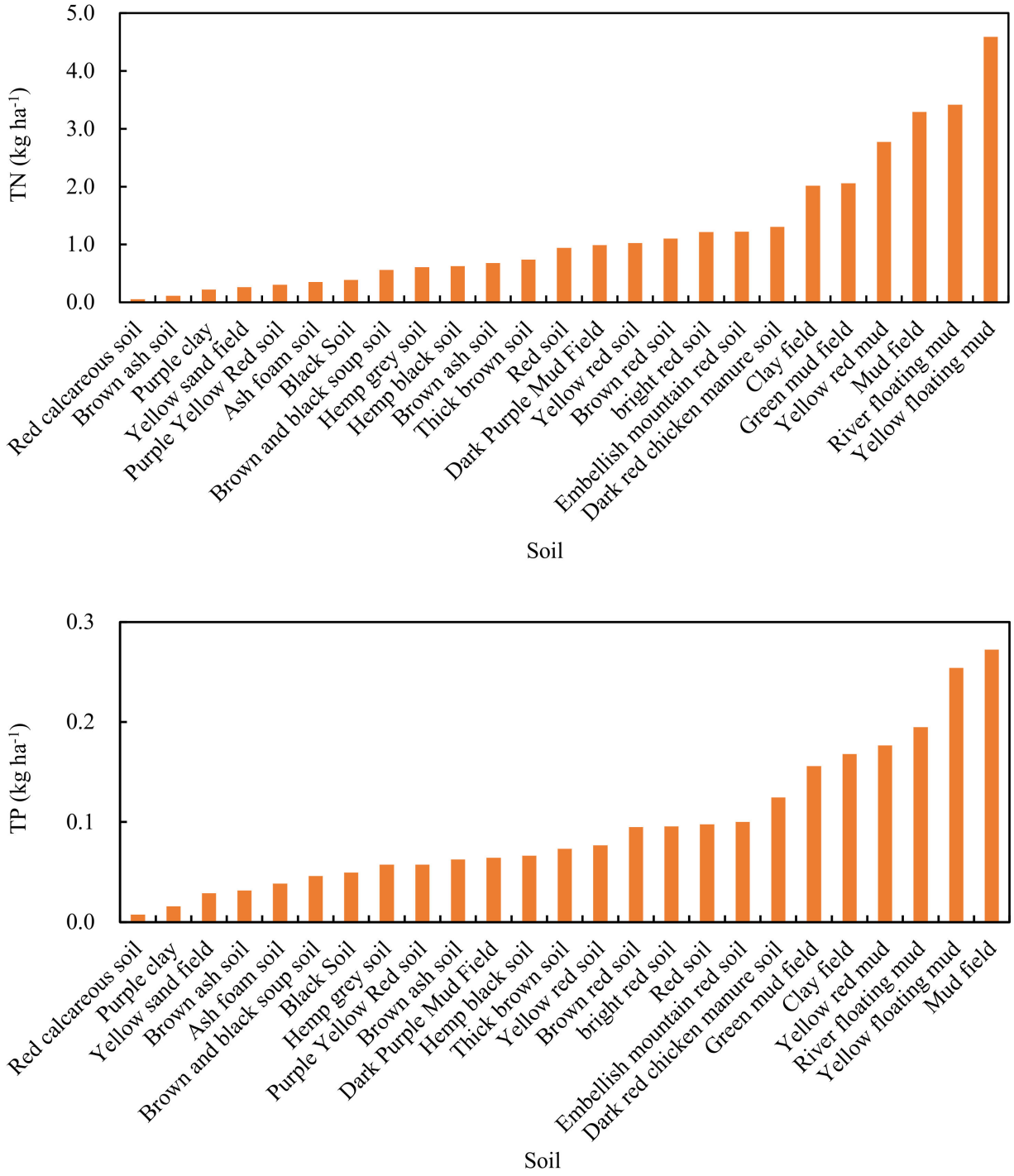


Figure 10. Pollution load intensity of different soil types in Lake Erhai watershed.

Forest land, grassland, and farmland occupied the largest parts of the study area, so these three land use types were selected for analysis. Figure 12 shows the distribution characteristics of the pollution load intensities of the same land use types with different slopes. For the farmland, the TN and TP pollution load intensities into the lake had a quadratic functional relationship with the slope, and the correlation coefficients reached 0.92 and 0.91, respectively. Moreover, with the increase in the slope, the TN and TP pollution load intensities showed a bowl-shaped trend. In the zone with a slope of 0–18°, the pollution load intensity negatively correlated with the slope. The reason is that in this zone, the dynamic and gravity effects of the slope on water flow were relatively weak, so the

phenomenon of water and soil loss was not obvious. In addition, the vegetation coverage formed by crops during the growth period impeded the erosion of soil by precipitation, and the crop roots could fix and utilize nutrients in the soil. Therefore, for the Erhai watershed, the zone with a slope of 0–18° was the optimal region for farming. In the zone with a slope of >18°, the pollution load intensity was positively correlated with the slope. The primary reason is that with the increase in the slope, the dynamic and gravity effects of slope on water flow surpassed the soil protection function of crops and the nutrient fixation function of roots. Furthermore, with the increase in precipitation, the phenomenon of water and soil loss could be aggravated, and a large amount of sediment and nutrients could be discharged into the river with surface runoff due to the slope. For the forest land and grassland, the TN and TP pollution load intensities into the lake exhibited a logarithmic functional relationship with the slope, and the correlation coefficient was around 0.80. With the increase in the slope, the pollution load intensity into the lake from the forest land and grassland decreased, which can be attributed to the weakening of the precipitation scouring, runoff peak value, and soil loss, as well as the formation of clear water runoff due to the functions of the forest and grassland.

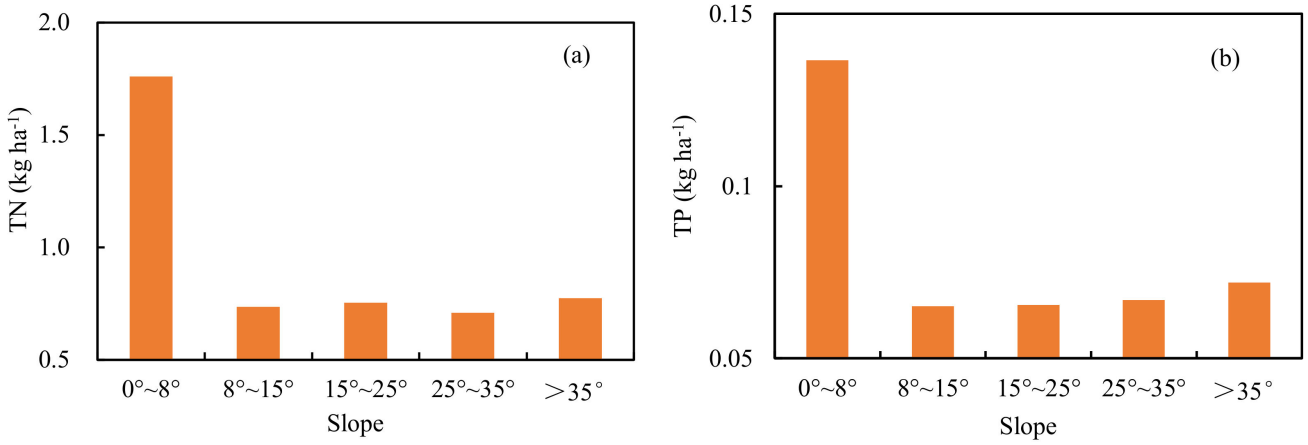


Figure 11. TN (**a**) and TP (**b**) pollution load intensity of different slope in Lake Erhai watershed.

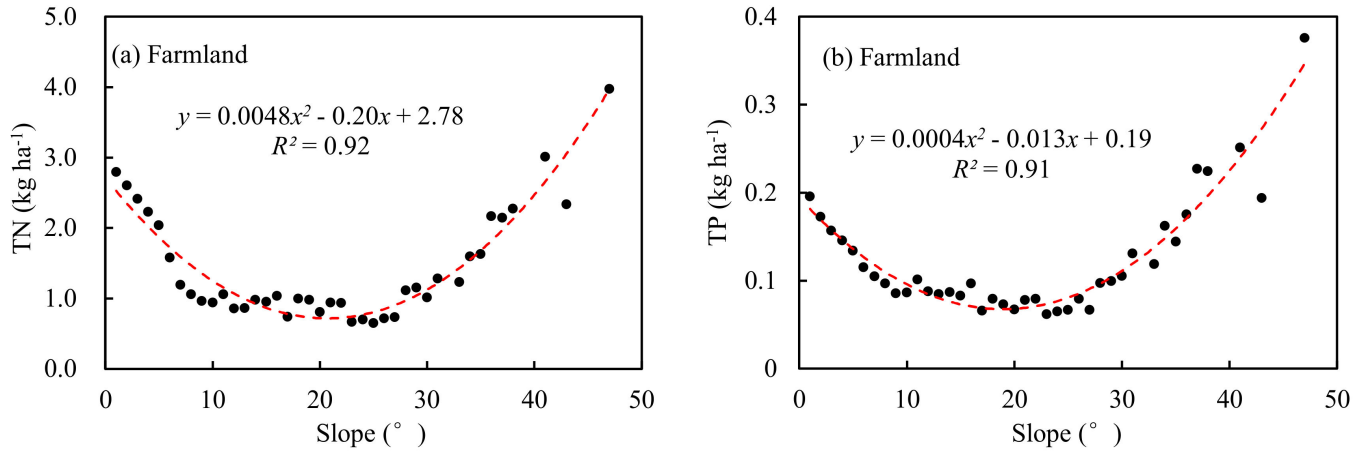


Figure 12. *Cont.*

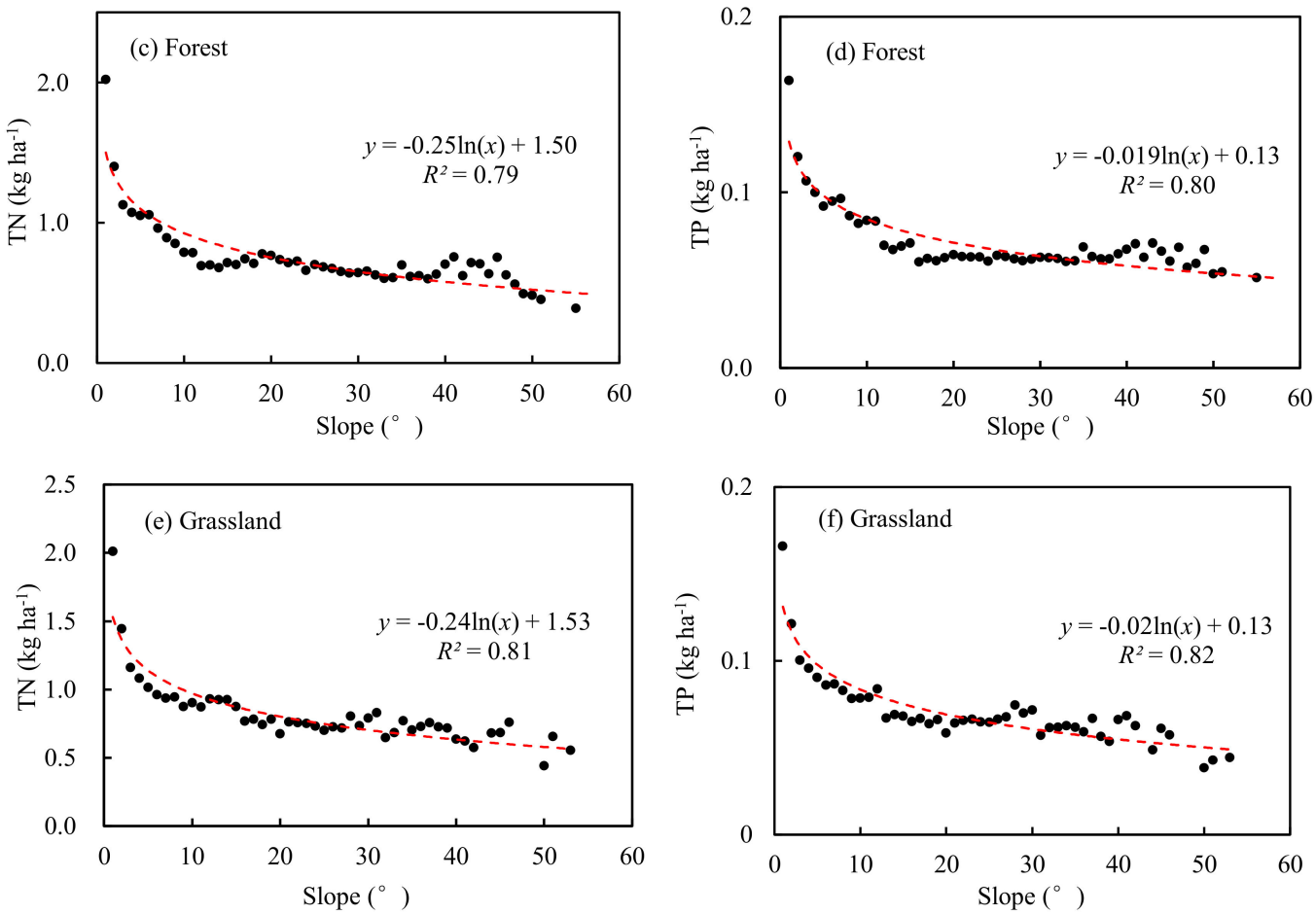


Figure 12. The distribution characteristics of the pollution load intensities of the same land use types with different slopes: TN for farmland (**a**), forest (**c**) and grassland (**e**), TP for farmland (**b**), forest (**d**) and grassland (**f**).

4.2.4. Elevation

In this study, the watershed was divided into different elevation zones at a geographical elevation interval of 100 m, and the TN and TP pollution load intensities into the lake in these elevation zones were analyzed. The results are shown in Figure 13. In the zone with geographical elevations < 2200 m, the average TN and TP pollution load intensities reached 1.61 and 0.12 kg/ha, respectively, which were 2.77 and 2.16 times the load intensities contributed from other elevation zones. The main reason for this phenomenon is that a large amount of farmland and residential construction land was concentrated in the zones with small geographical elevations, so the load was relatively large. In contrast, the forest land and grassland were concentrated in zones with large geographical elevations, and this load was relatively small. The influence of the geographical elevation on the nutrient load was further analyzed by investigating the pollution load intensities produced by the same land use type with different geographical elevations.

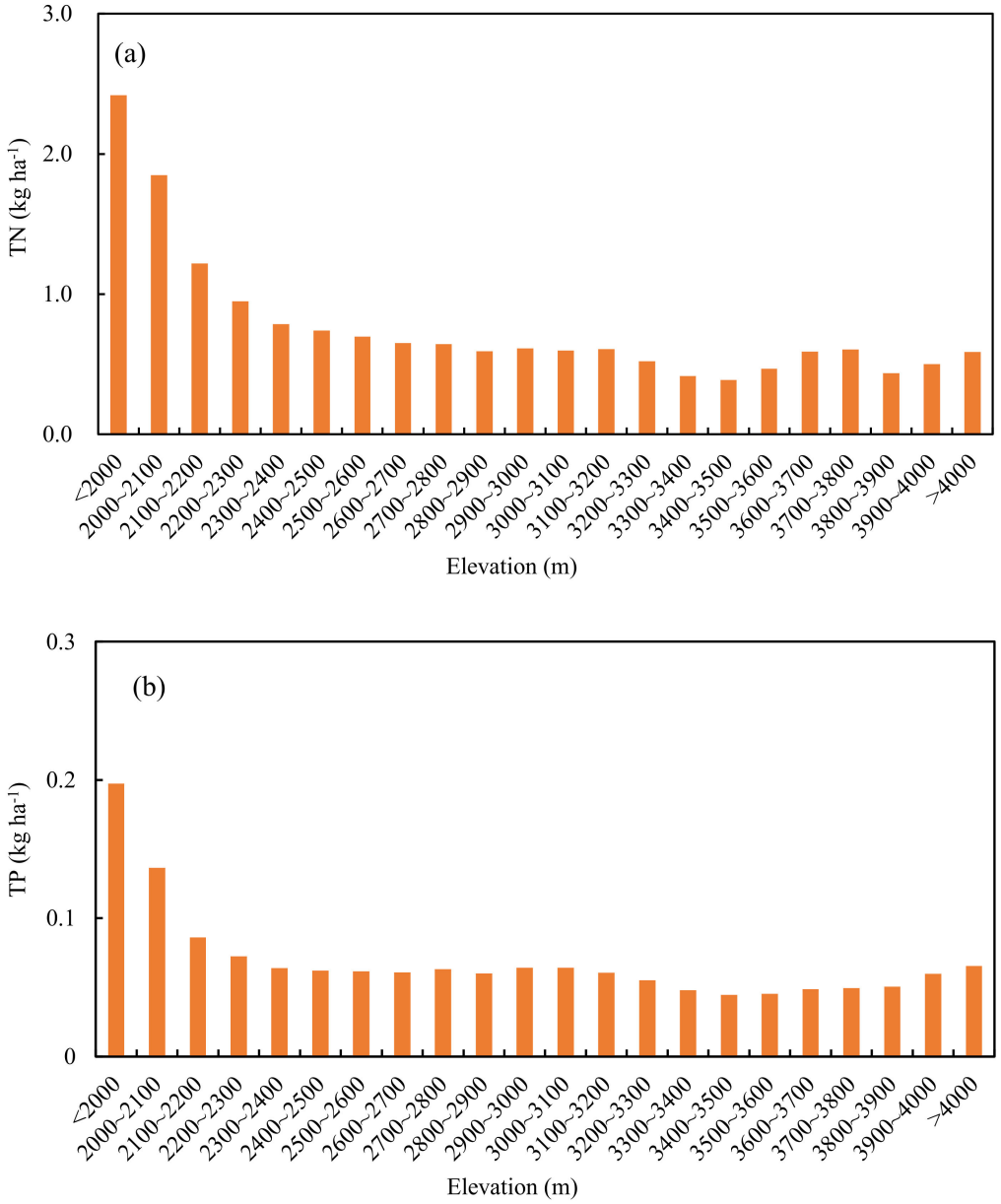


Figure 13. Intensity of TN (**a**) and TP (**b**) pollution load at different elevations in Lake Erhai watershed.

Similar to the study on pollution load intensities discharged into the lake from land with different slopes, the forest land, grassland, and farmland in the study area were selected as the research objects. Figure 14 shows the distribution of the load intensities contributed by the same land use type with different geographical elevations. In general, the load intensities of the farmland, forest land, and grassland exhibited a logarithmic functional relationship with the geographical elevation, and the correlation coefficient was greater than 0.77. With the increase in the geographical elevation, the load intensities into the lake from agricultural land, forest land, and grassland declined. The reasons are as follows: first, with the increase in the geographical elevation, the temperature decreased and irrigation costs increased, resulting in less farmland distribution in the zones with large elevations and relatively small pollution load. This reflects the effect of geographical elevation on the spatial distribution of the land use types in the watershed. Second, with the increase in geographical elevation, the precipitation increased. As the proportion of the area occupied by the forest land and grassland gradually increased, the pollution load

intensity into the lake declined correspondingly, thereby proving that the forest land and grassland could effectively impede and retain the pollutants. This reflects the functions of forests and grasslands in the conservation of the water source, pollution elimination, and clean water formation.

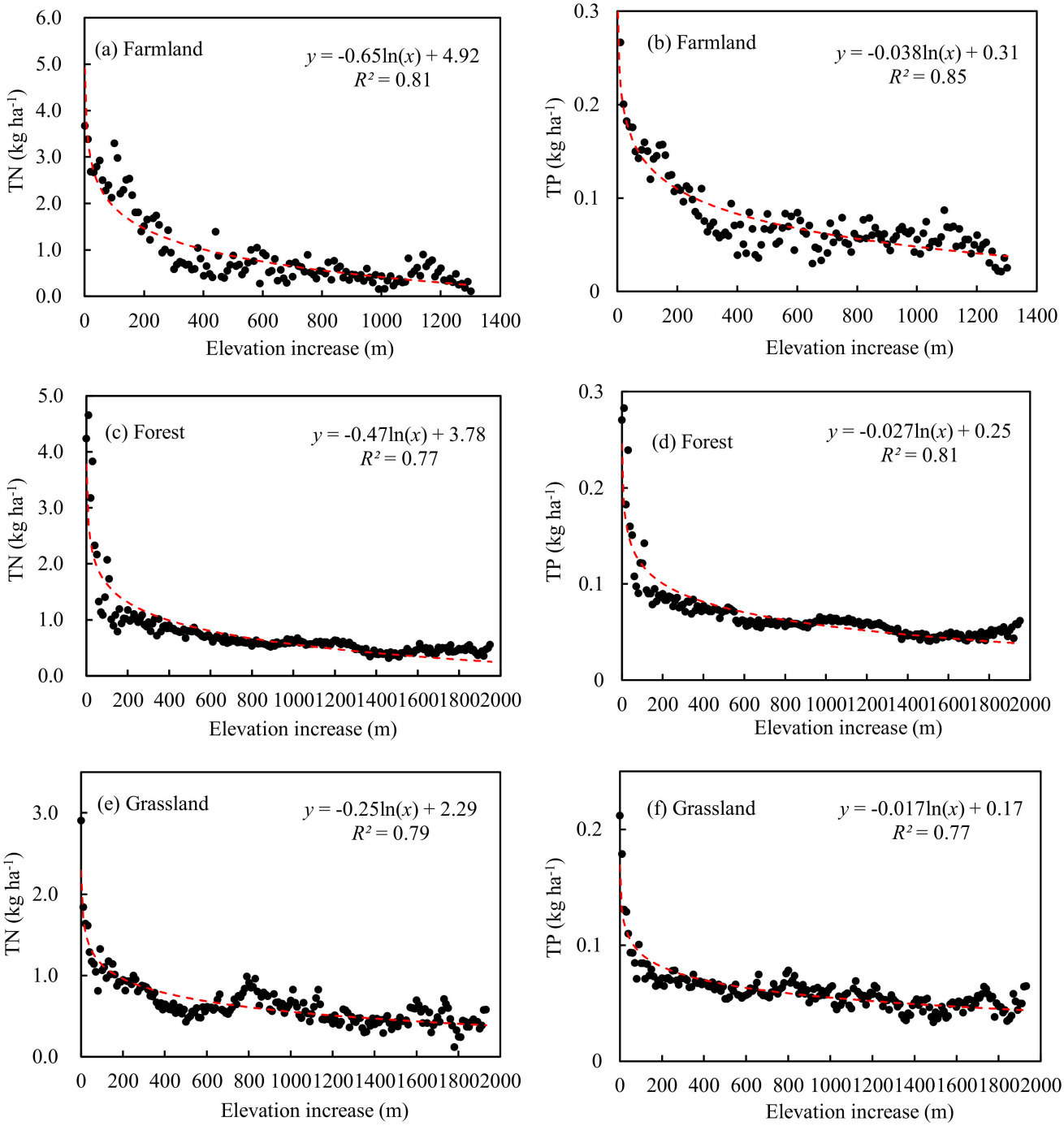


Figure 14. Variation characteristics of pollution load intensity at different elevations under a single land use type: TN for farmland (**a**), forest (**c**) and grassland (**e**), TP for farmland (**b**), forest (**d**) and grassland (**f**).

5. Conclusions

For an accurate understanding of the various characteristics of the non-point source pollution in the watershed, an MCAHP-based watershed dividing method was proposed. On this basis, for the first time, the SWPT method suitable for limited monitoring data and complex underlying surface conditions was established and applied to the Erhai Lake, a

typical plateau lake in China. Considering the characteristic spatial formula climate of the Erhai Lake watershed and the obvious spatial difference in the underlying surface conditions such as soil type, slope, and land use type, initially, the Erhai Lake watershed was divided into north, west, south, and east regions using the MCAHP method. The typical sub-watersheds in each division were then selected, and the hydrological and nutrient circulation simulations in these sub-watersheds were simulated with the SWAT model. Subsequently, the optimal parameters of all typical sub-watersheds were transplanted to the corresponding divisions for the simulation and evaluation of the pollution load of the whole watershed. Finally, the effects of different underlying surface conditions on the transport of non-point source pollution in the watershed were quantitatively studied, and the crucial topographic threshold values affecting the farming in the Erhai watershed were quantified.

The comparison of the SWPT- and AWPS-based simulation results showed that the simulation accuracy was significantly improved by 40% when the SWPT was adopted (YX: SWPT *Ens* = 0.88, while AWPS *Ens* = 0.43; BL: SWPT *Ens* = 0.87, while AWPS *Ens* = 0.62). Furthermore, the popularization of the SWPT was verified. The effects of the underlying surface conditions were studied, and the following conclusions were drawn:

1. The pollution load intensity of farmland into the lake was the largest due to artificial fertilization and other reasons. Paddy soil exhibited the largest total nitrogen and total phosphorus pollution load.
2. The pollution load intensity of agricultural land (dry land and paddy field) exhibited a quadratic functional relationship with the slope. The slope of 18° was a key topographic threshold for agricultural planting in the Erhai watershed. Therefore, in zones with slopes >18°, farming should be reduced as much as possible, and protective management measures such as terracing should be implemented.
3. The load intensities contributed by the forest land and grassland showed logarithmic functional relationships with the slope. The load intensity declined with the increase in slope. Therefore, in steep regions, afforestation, returning farmland to forest, and other projects should be extensively promoted.
4. The load intensities contributed from different land use types had logarithmic functional relationships with the geographical elevation. In the zones with geographical elevations smaller than 2000 m, the nitrogen and phosphorus pollution load intensities into the lake were relatively large, which were principally affected by the spatial distributions of farmland and residential construction land.

Author Contributions: X.L., G.H., and B.L. designed the project; X.C. processed the data, developed the methodology, performed the research, and wrote the manuscript; X.L., G.H., and W.P. provided overall guidance; F.D., A.H., W.W., and Q.L. collected the data and contributed to discussions and scientific advice. All authors have read and agreed to the published version of the manuscript.

Funding: This work was supported by the Joint Open Research Fund Program of State Key Laboratory of Hydroscience and Engineering and the Tsinghua–Ningxia Yinchuan Joint Institute of Internet of Waters on Digital Water Governance (No. sklhse-2019-Iow07), the National Key R&D Program of China (No. 2019YFC0409204, 2018YFC0407702), Beijing Natural Science Foundation (No. 8214064), and the basic Research Project of IWHR (No. WE0145B032021).

Data Availability Statement: Not applicable.

Conflicts of Interest: The authors declare no conflict of interest.

References

1. Hou, C.; Librada, M.; Botero-Acosta, A.; Guzman, J.A. Modeling field scale nitrogen non-point source pollution (NPS) fate and transport: Influences from land management practices and climate. *Sci. Total Environ.* **2020**, *759*, 143502. [CrossRef] [PubMed]
2. Ouyang, W.; Yang, W.; Tysklind, M.; Xu, Y.; Lin, C.; Gao, X.; Zhao, X. Using river sediments to analyze the driving force difference for non-point source pollution dynamics between two scales of watersheds. *Water Res.* **2018**, *139*, 311. [CrossRef] [PubMed]
3. Chen, L.; Zhong, Y.; Wei, G.; Cai, Y.; Shen, Z. Development of an integrated modeling approach for identifying multilevel non-point-source priority management areas at the watershed scale. *Water Resour. Res.* **2014**, *50*, 4095–4109. [CrossRef]

4. Han, D.; Currell, M.; Cao, G. Deep challenges for China's war on water pollution. *Environ. Pollut.* **2016**, *218*, 1222–1233. [CrossRef] [PubMed]
5. Srinivas, R.; Singh, A.; Dhadse, K.; Garg, C. An evidence based integrated watershed modelling system to assess the impact of non-point source pollution in the riverine ecosystem. *J. Clean. Prod.* **2020**, *246*, 118963. [CrossRef]
6. Qian, Y.; Sun, L.; Chen, D.; Liao, J.; Sun, Q. The response of the migration of non-point source pollution to land use change in a typical small watershed in a semi-urbanized area. *Sci. Total Environ.* **2021**, *785*, 147387. [CrossRef]
7. Zeng, J.; Huang, G.; Luo, H.; Mai, Y.; Wu, H. First flush of non-point source pollution and hydrological effects of LID in a Guangzhou community. *Sci. Rep.* **2019**, *9*, 13865. [CrossRef]
8. Zhang, T.; Yang, Y.; Ni, J.; Xie, D. Construction of an integrated technology system for control agricultural non-point source pollution in the Three Gorges Reservoir Areas. *Agric. Ecosyst. Environ.* **2020**, *295*, 106919. [CrossRef]
9. Chen, L.; Chen, S.; Li, S.; Shen, Z. Temporal and spatial scaling effects of parameter sensitivity in relation to non-point source pollution simulation. *J. Hydrol.* **2019**, *571*, 36–49. [CrossRef]
10. Ouyang, W.; Hao, F.; Shi, Y.; Gao, X.; Gu, X.; Lian, Z. Predictive ability of climate change with the automated statistical downscaling method in a freeze-thaw agricultural area. *Clim. Dyn.* **2019**, *52*, 7013–7028. [CrossRef]
11. Wan, W.; Han, Y.; Wu, H.; Liu, F.; Liu, Z. Application of the source–sink landscape method in the evaluation of agricultural non-point source pollution: First estimation of an orchard-dominated area in China. *Agric. Water Manag.* **2021**, *252*, 106910. [CrossRef]
12. Xue, L.; Hou, P.; Zhang, Z.; Shen, M.; Yang, L. Application of systematic strategy for agricultural non-point source pollution control in Yangtze River basin, China. *Agric. Ecosyst. Environ.* **2020**, *304*, 107148. [CrossRef]
13. Tao, Y.; Liu, J.; Guan, X.; Chen, H.; Ji, M. Estimation of potential agricultural non-point source pollution for Baiyangdian Basin, China, under different environment protection policies. *PLoS ONE* **2020**, *15*, e0239006. [CrossRef] [PubMed]
14. Luo, X.; Wu, W.; He, D.; Li, Y.; Ji, X. Hydrological Simulation Using TRMM and CHIRPS Precipitation Estimates in the Lower Lancang-Mekong River Basin. *Chin. Geogr. Sci.* **2019**, *29*, 13–25. [CrossRef]
15. Chen, X.; Liu, X.; Peng, W.; Dong, F.; Huang, Z.; Wang, R. Non-Point Source Nitrogen and Phosphorus Assessment and Management Plan with an Improved Method in Data-Poor Regions. *Water* **2017**, *10*, 17. [CrossRef]
16. Maringanti, C.; Chaubey, I.; Arabi, M.; Engel, B. Application of a multi-objective optimization method to provide least cost alternatives for NPS pollution control. *Environ. Manag.* **2011**, *48*, 448–461. [CrossRef]
17. Nilawar, A.; Waikar, M. Impacts of climate change on streamflow and sediment concentration under RCP 4.5 and 8.5: A case study in Purna river basin, India. *Sci. Total Environ.* **2019**, *650*, 2685–2696. [CrossRef]
18. Daniel, B.; Tena, A.; Asfaw, K.; Gete, Z.; Assefa, M. Modeling Climate Change Impact on the Hydrology of Keleta Watershed in the Awash River Basin, Ethiopia. *Environ. Modeling Assess.* **2018**, *24*, 1–13.
19. Wen, X.; Liu, Z.; Lei, X.; Lin, R.; Fang, G.; Tan, Q.; Wang, C.; Tian, Y.; Quan, J. Future changes in Yuan River ecohydrology: Individual and cumulative impacts of climates change and cascade hydropower development on runoff and aquatic habitat quality. *Sci. Total Environ.* **2018**, *633*, 1403. [CrossRef]
20. Peraza-Castro, M.; Ruiz-Romera, E.; Meaurio, M.; Sauvage, S.; Sánchez-Pérez, J. Modelling the impact of climate and land cover change on hydrology and water quality in a forest watershed in the Basque Country (Northern Spain). *Ecol. Eng.* **2018**, *122*, 315–326. [CrossRef]
21. Rui, Y.; Zhang, X.; Yan, S.; Zhang, J.; Hao, C. Spatial patterns of hydrological responses to land use/cover change in a catchment on the Loess Plateau, China. *Ecol. Indic.* **2018**, *92*, 151–160.
22. Hyandye, C.; Worqul, A.; Martz, L.; Muzuka, A. The impact of future climate and land use/cover change on water resources in the Ndembera watershed and their mitigation and adaptation strategies. *Environ. Syst. Res.* **2018**, *7*, 7. [CrossRef]
23. Kaandorp, V.; Molina-Navarro, E.; Andersen, H.; Bloomfield, J.; Kuijper, M.; Louw, P. A conceptual model for the analysis of multi-stressors in linked groundwater–surface water systems. *Sci. Total Environ.* **2018**, *627*, 880–895. [CrossRef] [PubMed]
24. Hoang, L.; Schneiderman, E.; Moore, K.; Mukundan, R.; Owens, E.; Steenhuis, T. Predicting saturation-excess runoff distribution with a lumped hillslope model: SWAT-HS. *Hydrol. Process.* **2017**, *31*, 2226–2243. [CrossRef]
25. Hu, S.; Yang, D.; Wu, J.; Gao, Y.; Qiu, H.; Cao, M.; Song, J.; Wan, H. Spatio-temporal Variation Characteristics of Baseflow in the Bahe River Basin Based on Digital Filter Method and SWAT Model. *Sci. Geogr. Sin.* **2017**, *37*, 455–463.
26. Foteh, R.; Garg, V.; Nikam, B.; Khadatare, M.; Aggarwal, S.; Kumar, A. Reservoir Sedimentation Assessment through Remote Sensing and Hydrological Modelling. *J. Indian Soc. Remote Sens.* **2018**, *46*, 1893–1905. [CrossRef]
27. Mohammad, H.; Assefa, M.; Hector, F. Erosion and Sediment Transport Modelling in Shallow Waters: A Review on Approaches, Models and Applications. *Int. J. Environ. Res. Public Health* **2018**, *15*, 518.
28. Le Roux, J. Sediment Yield Potential in South Africa's Only Large River Network without a Dam: Implications for Water Resource Management: Sediment Yield in South Africa's Only Large River without a Dam. *Land Degrad. Dev.* **2018**, *29*, 765–775. [CrossRef]
29. Zeiger, S.; Hubbart, J. A SWAT model validation of nested-scale contemporaneous stream flow, suspended sediment and nutrients from a multiple-land-use watershed of the central USA. *Sci. Total Environ.* **2016**, *572*, 232–243. [CrossRef]
30. Özcan, Z.; Kentel, E.; Alp, E. Determination of unit nutrient loads for different land uses in wet periods through modelling and optimization for a semi-arid region. *J. Hydrol.* **2016**, *540*, 40–49. [CrossRef]
31. Alemayehu, T.; Griensven, A.; Woldegiorgis, B.; Bauwens, W. An improved SWAT vegetation growth module and its evaluation for four tropical ecosystems. *Hydrol. Earth Syst. Sci.* **2017**, *21*, 4449–4467. [CrossRef]

32. Zhao, F.; Wu, Y.; Qiu, L.; Sivakumar, B.; Zhang, F.; Sun, Y. Spatio-temporal features of the hydro-biogeochemical cycles in a typical loess gully watershed. *Ecol. Indic.* **2018**, *91*, 542–554. [CrossRef]
33. Evenson, G.; Golden, H.; Lane, C.; Mclaughlin, D.; D'Amico, E. Depressional Wetlands Affect Watershed Hydrological, Biogeochemical, and Ecological Functions. *Ecol. Appl.* **2018**, *28*, 953–966. [CrossRef]
34. Ni, X.; Parajuli, P. Evaluation of the impacts of BMPs and tailwater recovery system on surface and groundwater using satellite imagery and SWAT reservoir function. *Agric. Water Manag.* **2018**, *210*, 78–87. [CrossRef]
35. Imani, S.; Niksokhan, M.; Jamshidi, S.; Abbaspour, K. Discharge permit market and farm management nexus: An approach for eutrophication control in small basins with low-income farmers. *Environ. Monit. Assess.* **2017**, *189*, 346. [CrossRef] [PubMed]
36. Ouyang, W.; Hao, F.; Wang, X.; Cheng, H. Nonpoint Source Pollution Responses Simulation for Conversion Cropland to Forest in Mountains by SWAT in China. *Environ. Manag.* **2008**, *41*, 79–89. [CrossRef] [PubMed]
37. Shen, Z.; Chen, L.; Hong, Q.; Qiu, J.; Xie, H.; Liu, R. Assessment of nitrogen and phosphorus loads and causal factors from different land use and soil types in the Three Gorges Reservoir Area. *Sci. Total Environ.* **2013**, *454–455*, 383–392. [CrossRef]
38. Shen, Z.; Chen, L.; Hong, Q.; Xie, H.; Qiu, J.; Liu, R. Vertical Variation of Nonpoint Source Pollutants in the Three Gorges Reservoir Region. *PLoS ONE* **2013**, *8*, e71194. [CrossRef]
39. Ge, Y.; Xue, B.; Lai, G.; Feng, G.; Liu, X. A 200-year historical modeling of catchment nutrient changes in Taihu basin, China. *Hydrobiologia* **2007**, *581*, 79–87.
40. Kenea, U.; Adeba, D.; Regasa, M.S.; Nones, M. Hydrological Responses to Land Use Land Cover Changes in the Fincha'a Watershed, Ethiopia. *Land* **2021**, *10*, 916. [CrossRef]
41. Cibin, R.; Sudheer, K.; Chaubey, I. Sensitivity and identifiability of stream flow generation parameters of the SWAT model. *Hydrol. Process.* **2010**, *24*, 1133–1148. [CrossRef]
42. Herman, J.; Kollat, J.; Reed, P.; Wagener, T. Technical Note: Method of Morris effectively reduces the computational demands of global sensitivity analysis for distributed watershed models. *Hydrol. Earth Syst. Sci.* **2013**, *17*, 2893–2903. [CrossRef]
43. Guse, B.; Pfannerstill, M.; Kiesel, J.; Strauch, M.; Fohrer, N. Analysing spatio-temporal process and parameter dynamics in models to characterise contrasting catchments. *J. Hydrol.* **2019**, *570*, 863–874. [CrossRef]
44. Chen, Y.; Marek, G.; Marek, T.; Porter, D.; Srinivasan, R. Simulating the effects of agricultural production practices on water conservation and crop yields using an improved SWAT model in the Texas High Plains, USA. *Agric. Water Manag.* **2021**, *244*, 106574. [CrossRef]
45. Cheng, Y.; Ao, T.; Li, X.; Wu, B. Runoff simulation by SWAT model based on parameters transfer method in ungauged catchments of middle reaches of Jialing River. *Trans. Chin. Soc. Agric. Eng.* **2016**, *32*, 81–86.
46. Wu, B.; Li, X.; Ao, T.; Fan, Y.; Wang, X. Study of SWAT Model Based on Parameter Transfer Method in Data Scarce Catchment for Non-point Source Pollution Simulation. *J. Sichuan Univ. (Eng. Sci. Ed.)* **2015**, *47*, 9–16.
47. Hong, Q.; Sun, Z.; Chen, L.; Liu, R.; Shen, Z. Small-scale watershed extended method for non-point source pollution estimation in part of the Three Gorges Reservoir Region. *Int. J. Environ. Sci. Technol.* **2012**, *9*, 595–604. [CrossRef]
48. Shang, X.; Wang, X.; Zhang, D.; Chen, W.; Chen, X.; Kong, H. An improved SWAT-based computational framework for identifying critical source areas for agricultural pollution at the lake basin scale. *Ecol. Model.* **2012**, *226*, 1–10. [CrossRef]
49. Wang, S. *Eutrophication Process and Mechanism of Erhai Lake*; Science Press: Beijing, China, 2015.
50. Li, Y.; Wang, C.; Tang, H. Research advances in nutrient runoff on sloping land in watersheds. *Aquat. Ecosyst. Health Manag.* **2006**, *9*, 27–32. [CrossRef]
51. Yang, G.; Best, E.; Whiteaker, T.; Teklitz, A.; Yeghiazarian, L. A screening-level modeling approach to estimate nitrogen loading and standard exceedance risk, with application to the Tippecanoe River watershed, Indiana. *J. Environ. Manag.* **2014**, *135*, 1–10. [CrossRef] [PubMed]
52. Li, Y.; Li, B.; Zhang, K.; Zhu, J.; Yang, Q. Study on spatiotemporal distribution characteristics of annual precipitation of Erhai Basin. *J. China Inst. Water Resour. Hydropower Res.* **2017**, *15*, 234–240.
53. McGrath, S.; Zhao, X.; Steele, R.; Thombs, B.; Benedetti, A.; DEPRESSED Collaboration. Estimating the sample mean and standard deviation from commonly reported quantiles in meta-analysis. *Stat. Methods Med. Res.* **2020**, *29*, 2520–2537. [CrossRef] [PubMed]
54. Dahri, N.; Abida, H. Monte Carlo simulation-aided analytical hierarchy process (AHP) for flood susceptibility mapping in Gabes Basin (southeastern Tunisia). *Environ. Earth Sci.* **2017**, *76*, 302. [CrossRef]